Available online at www.sciencedirect.com
ScienceDirect
Journal of Sound and Vibration 303 (2007) 832–857
JOURNAL OF SOUND AND VIBRATION
www.elsevier.com/locate/jsvi

Dynamic lateral torsional post-buckling of a beam–mass system: Theory

O. Yogev, M.B. Rubin*, I. Bucher

Faculty of Mechanical Engineering, Technion—Israel Institute of Technology, 32000 Haifa, Israel

Received 25 August 2006; received in revised form 29 January 2007; accepted 6 February 2007
Available online 2 April 2007

Abstract

In this paper, the theory of a Cosserat point is used as a numerical model of a nonlinear elastic beam–mass system and simulations of dynamic lateral torsional buckling are compared with results of experiments. The Cosserat equations are solved using the Newmark time-integration scheme and an analytical expression for the tangent stiffness of the resulting Newton–Raphson iteration procedure is developed. Also, the effects of material damping, aerodynamic drag and gravity have been included. The simulations reproduce the experimental result that two different nonlinear modes of vibration occur at the same excitation amplitude and frequency. One mode: Torsion I is a post-buckling mode associated with out-of-plane motion of the beam–mass system, which is dominated by oscillating torsion of the beam. The second mode: Bending II is dominated by a nonlinear second bending mode in the weak bending plane. The simulations of Torsion I and Bending II and another mode Torsion II are in reasonably good quantitative agreement with the experimental results. However, the model is not able to accurately simulate the response of Torsion III (which was similar to Torsion I and II but with a larger amplitude of vibration). Comparison is also made with the commercial code ANSYS.

1. Introduction

In Ref. [1], an experimental setup was designed to produce dynamic lateral torsional buckling of a beam–mass system. Fig. 1 shows a sketch of the beam–mass system with $\mathbf{e}_i$ $(i = 1, 2, 3)$ being fixed rectangular Cartesian base vectors. Specifically, an elastic beam of mass m, length L, and rectangular cross-section with height h and width w, was clamped at one end to a block that was attached to a motor shaft. The distance between the clamped end of the block and the axis of the motor was R. The other end of the beam was clamped to a rectangular block of mass M, with length B, height H and width W. The motor shaft was controlled to oscillate with angle ϕ, such that

$$\phi(t) = \phi_0 \sin(\omega t), \tag{1}$$

where ϕ_0 is the amplitude and ω the frequency. For small amplitudes, the motor merely causes the beam–mass system to oscillate in the plane of stiffest bending of the beam. However, it was shown that for a range of

*Corresponding author. Fax: +972 4 829 5711.
E-mail address: mbrubin@tx.technion.ac.il (M.B. Rubin).

0022-460X/$ - see front matter © 2007 Elsevier Ltd. All rights reserved.
doi:10.1016/j.jsv.2007.02.009

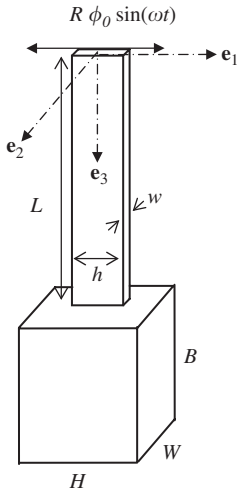

Fig. 1. Sketch of the beam–mass system.

amplitudes and frequencies, dynamic buckling occurs with the beam bending out-of-plane, the mass remaining on one side of the vertical ($\mathbf{e}_1$–$\mathbf{e}_3$) plane and with the mass oscillating so that it applies torsion to the beam. This buckling phenomena characterizes the responses of Torsions I, II and III described in Ref. [1], which occurred, respectively, for ($\phi_0 = 0.65°$, $\omega = 35.0\,\text{Hz}$), ($\phi_0 = 1.50°$, $\omega = 27.0\,\text{Hz}$) and ($\phi_0 = 1.49°$, $\omega = 25.5\,\text{Hz}$). In addition, it was shown that two different modes of vibration occur at the same excitation amplitude and frequency associated with Torsion I. In particular, the second mode Bending II is dominated by second mode bending in the weak plane of bending of the beam which is accommodated by torsion of the beam.

In Ref. [1], parametric functions were presented, which quantify the time response of the motion of the beam's centerline at a number of deformed axial locations and the torsion angle at the beam's end for the four responses Torsions I–III, and Bending II. Also, polynomial functions were presented to characterize the spatial shape of the beam's centerline at a number of times for these four responses. Measurements were made of the first four natural frequencies and their associated damping coefficients and for the effect of gravity on the first bending mode in the weak bending plane. This provides substantial data to test the accuracy of mathematical and numerical models predicting this nonlinear dynamic phenomena.

Nonlinear theories of rods have been developed [2,3], which include bending, torsion, axial extension and tangential shear deformation, but which model the cross-section of the rod as rigid. More general nonlinear theories of a Cosserat curve have been developed [4,5] which, in addition, allow for normal extension and shear deformations in the cross-section of the rod. Also, it is noted that the nonlinear dynamic response of a cantilever beam with a tip mass has been considered in Ref. [6]. However, that work [6] is not directly applicable to the problem under consideration here since there the tip mass was modeled as a point mass and not a finite block and forced vibrations were not considered.

A finite element for large deformations of rods with rigid cross-sections has been developed [7–9] using the formulation [10] which was based on that in Ref. [2]. More recently [11–13], a finite element based on the theory of a Cosserat point has been developed which includes all of the kinematics modeled by the theory of a Cosserat curve [4,5]. In particular, the theory of a Cosserat point has been developed [11,12] to formulate the solution of dynamic problems of nonlinear elastic beams. This theory includes both material and geometric nonlinearities and it has been tested for static torsional buckling [13], for static buckling of a shallow arch [14], and for small deformation vibrations of circular arches [15]. The objective of this paper is to further test the accuracy of this Cosserat theory for a complicated nonlinear dynamic problem of rods. Comparison is also made with the commercial code ANSYS.

An outline of the paper is as follows. Section 2 presents a summary of the equations of the theory of a Cosserat point for rods. Section 3 describes the problem formulation and Section 4 discusses the Newmark scheme used to integrate the ordinary differential equations in time. Section 5 presents the linearized equations

of motion and discusses the procedure for determining the damping coefficients. A preliminary example problem is considered in Section 6 to study the accuracy of the numerical scheme and comparisons of the simulations with the experimental data are given in Section 7. Section 8 shows a comparison with the commercial code ANSYS and conclusions are presented in Section 9. Also, Appendix A presents details of the determination of the analytical form of the tangent stiffness used in the Newmark integration scheme.

Throughout the text, bold-faced symbols are used to denote vector and tensor quantities. Also, $\mathbf{I}$ denotes the unity tensor; $\mathrm{tr}(\mathbf{A})$ denotes the trace of the second-order tensor $\mathbf{A}$; $\mathbf{A}^{\mathrm{T}}$ denotes the transpose of $\mathbf{A}$; $\mathbf{A}^{-1}$ denotes the inverse of $\mathbf{A}$; $\mathbf{A}^{-\mathrm{T}}$ denotes the inverse of the transpose of $\mathbf{A}$; and $\det(\mathbf{A})$ denotes the determinant of $\mathbf{A}$. The scalar $\mathbf{a}\cdot\mathbf{b}$ denotes the dot product between two vectors $\mathbf{a},\mathbf{b}$; the scalar $\mathbf{A}\cdot\mathbf{B}=\mathrm{tr}(\mathbf{A}\mathbf{B}^{\mathrm{T}})$ denotes the dot product between two second order tensors $\mathbf{A},\mathbf{B}$; the vector $\mathbf{a}\times\mathbf{b}$ denotes the cross product between $\mathbf{a}$ and $\mathbf{b}$; and the second order tensor $\mathbf{a}\otimes\mathbf{b}$ denotes the tensor product between $\mathbf{a}$ and $\mathbf{b}$. The range of Greek indices always being $(1,2)$, the range of Latin indices can be $(0,1,2)$, $(1,2,3)$ or $(0,1,\ldots,5)$ and will be specified when it is not clear from the context. Also, the summation convention over repeated indices in suspended throughout the text.

2. Summary of the equations of a Cosserat point

The objective of this section is to summarize the main equations of the theory of a Cosserat point, which were developed to formulate the numerical solution of dynamic problems of elastic rods. Details of these equations can be found in Refs. [11,12,16]. In order to simulate the experiments in Ref. [1], it is sufficient to confine attention to the specialized theory for a beam, which is straight in its unstressed reference configuration. The beam is divided into N elements and the Ith element ($I=1,\ldots,N$) is modeled using the theory of a Cosserat point. The equations of motion of the entire beam are obtained by using kinematic and kinetic coupling conditions at the common boundaries of the elements. These coupling equations yield a set of ordinary differential equations, which are functions of time t only.

The theory of a Cosserat point can be developed by averaging the three-dimensional equations or by the direct approach. In either case, the constitutive equations in the Cosserat theory are developed by the direct approach. Within the context of the direct approach, the Ith nodal cross-section is characterized by the three constant nodal directors ${}_I\mathbf{D}_i^*$ ($i=0,1,2$) in the unstressed reference configuration and by the nodal directors ${}_I\mathbf{d}_i^*(t)$ ($i=0,1,2$) in the deformed present configuration, which are functions of time t only. The vectors $\{{}_I\mathbf{D}_0^*,{}_I\mathbf{d}_0^*\}$ locate the centroid of the cross-section relative to a fixed origin and the vectors $\{{}_I\mathbf{D}_1^*,{}_I\mathbf{d}_1^*\}$ and $\{{}_I\mathbf{D}_2^*,{}_I\mathbf{d}_2^*\}$ are identified with two independent line elements which determine the beam's cross-section. The dynamical equations for the motion of the entire beam are a set of $3(N+1)$ vector second-order ordinary differential equations of time only to determine the $3(N+1)$ nodal vectors ${}_I\mathbf{d}_i^*$ ($I=1,2,\ldots,N+1$; $i=0,1,2$). Fig. 2 shows the deformed beam–mass system associated with a solution of the nonlinear equations for the response Torsion I in Ref. [1]. The arrows in this figure represent the nodal directors $\{{}_I\mathbf{d}_1^*,{}_I\mathbf{d}_2^*\}$, which characterize the element's cross-sections.

The constitutive equations for the Ith element are written in terms of kinematic quantities defined by the reference element directors ${}_I\mathbf{D}_i$ ($i=0,1,\ldots,5$) and the present element directors ${}_I\mathbf{d}_i(t)$ ($i=0,1,\ldots,5$), which are both related to the nodal directors by equations of the forms

$$
{}_I\mathbf{d}_i=\frac{1}{2}\left[{}_I\mathbf{d}_i^*+{}_{I+1}\mathbf{d}_i^*\right],\quad {}_I\mathbf{d}_{3+i}=\frac{1}{{}_IL}\left[-{}_I\mathbf{d}_i^*+{}_{I+1}\mathbf{d}_i^*\right]
$$
$$
i=0,1,2 \tag{2}
$$

with ${}_I\mathbf{d}_i$ replaced by ${}_I\mathbf{D}_i$ and ${}_I\mathbf{d}_i^*$ replaced by ${}_I\mathbf{D}_i^*$ for the reference directors. Also, the height ${}_IH$, width ${}_IW$ and length ${}_IL$ of the Ith element in its reference configuration are defined so that

$$
|{}_I\mathbf{D}_1|=1,\quad |{}_I\mathbf{D}_2|=1,\quad |{}_I\mathbf{D}_3|=1. \tag{3}
$$

Moreover, the directors are defined so that $\{{}_I\mathbf{D}_1,{}_I\mathbf{D}_2,{}_I\mathbf{D}_3\}$ and $\{{}_I\mathbf{d}_1,{}_I\mathbf{d}_2,{}_I\mathbf{d}_3\}$ each are linearly independent sets

$$
{}_ID^{1/2}={}_I\mathbf{D}_1\times{}_I\mathbf{D}_2\cdot{}_I\mathbf{D}_3>0,\quad {}_Id^{1/2}={}_I\mathbf{d}_1\times{}_I\mathbf{d}_2\cdot{}_I\mathbf{d}_3>0. \tag{4}
$$

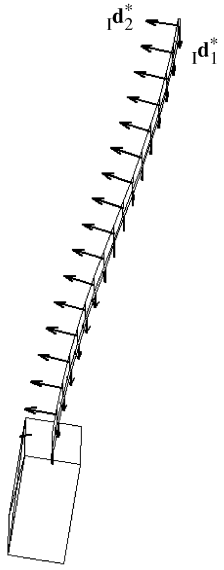

Fig. 2. Torsion I: The deformed beam and mass showing arrows associated with the nodal directors $\{{}_I\mathbf{d}_1^*, {}_I\mathbf{d}_2^*\}$, which characterize the element cross-sections.

Also, the element director velocities ${}_I\mathbf{w}_i$ are specified by

$$ {}_I\mathbf{w}_i = {}_I\dot{\mathbf{d}}_i \quad i = 0, 1, \ldots, 5, \tag{5} $$

where a superposed dot denotes time differentiation.

In addition, the Cosserat point is characterized by its inertia properties

$$ \left\{ {}_Im, {}_Iy^{ij} = {}_Iy^{ji},\ {}_I\dot{y}^{ij} = 0 \right\} \quad \text{for } i,j = 0, 1, \ldots, 5, \tag{6} $$

where ${}_Im$ is the mass of the element and ${}_Iy^{ij}$ are the constant director inertia coefficients. Then, the conservation of mass and the balances of director momentum can be written in the forms

$$ {}_I\dot{m} = 0, \quad \frac{\mathrm{d}}{\mathrm{d}t}\left[\sum_{j=0}^{5} {}_Im_I y^{ij}\, {}_I\mathbf{w}_j\right] = {}_Im_I\mathbf{b}^i - {}_I\mathbf{t}^i \quad \text{for } i = 0, 1, \ldots, 5 \tag{7} $$

with

$$ {}_I\mathbf{t}^0 = 0,\ {}_Im_I\mathbf{b}^i = {}_Im_I\mathbf{B}^i + {}_I\mathbf{m}_1^i + {}_I\mathbf{m}_2^i \quad \text{for } i = 0, 1, \ldots, 5. \tag{8} $$

In these equations, ${}_I\mathbf{B}^i$ are the specific (per unit mass) external assigned director couples due to body force and tractions on the lateral surface of the element, ${}_I\mathbf{m}_1^i$ and ${}_I\mathbf{m}_2^i$ are the director couples applied to the ends I and $(I+1)$, respectively, and ${}_I\mathbf{t}^i$ are intrinsic director couples, which need to be specified by constitutive equations. Moreover, by introducing the second-order tensor ${}_I\mathbf{T}$, the reduced form of the balance of angular momentum becomes

$$ {}_I\mathbf{T} = {}_Id^{-1/2}\sum_{i=1}^{5} {}_I\mathbf{t}^i \otimes {}_I\mathbf{d}_i = {}_I\mathbf{T}^{\mathrm{T}}. \tag{9} $$

In order to develop constitutive equations for nonlinear elastic elements it is convenient to introduce the reciprocal vectors ${}_I\mathbf{D}^i$ and ${}_I\mathbf{d}^i$, such that

$$ {}_I\mathbf{D}_i \cdot {}_I\mathbf{D}^j = \delta_i^j,\ {}_I\mathbf{d}_i \cdot {}_I\mathbf{d}^j = \delta_i^j \quad \text{for } i,j = 1, 2, 3, \tag{10} $$

where δ_i^j is the Kronecker delta symbol. Then, the non-singular deformation tensor ${}_I\mathbf{F}$, its determinant ${}_IJ$, the deformation tensors ${}_I\mathbf{C}$ and ${}_I\mathbf{B}$, and the inhomogeneous strains ${}_I\boldsymbol{\beta}_\alpha$ are defined by the formulas

$$
\begin{aligned}
&{}_I\mathbf{F} = \sum_{i=1}^{3} {}_I\mathbf{d}_i \otimes {}_I\mathbf{D}^i, \quad {}_IJ = \det({}_I\mathbf{F}) = \frac{{}_Id^{1/2}}{{}_ID^{1/2}} > 0, \quad {}_I\mathbf{C} = {}_I\mathbf{F}^{\mathrm{T}}\,{}_I\mathbf{F}, \quad {}_I\mathbf{B} = {}_I\mathbf{F}\,{}_I\mathbf{F}^{\mathrm{T}},\\
&{}_I\boldsymbol{\beta}_\alpha = {}_I\mathbf{F}^{-1}\,{}_I\mathbf{d}_{3+\alpha} - {}_I\mathbf{D}_{3+\alpha} \quad \text{for } \alpha = 1,2.
\end{aligned}
\tag{11}
$$

Also, the deformation rate tensor ${}_I\mathbf{L}$, its symmetric part ${}_I\mathbf{D}$ and its skew-symmetric part ${}_I\mathbf{W}$ are defined by

$$
\begin{aligned}
&{}_I\mathbf{L} = {}_I\dot{\mathbf{F}}\,{}_I\mathbf{F}^{-1} = \sum_{i=1}^{3} {}_I\mathbf{w}_i \otimes {}_I\mathbf{d}^i = {}_I\mathbf{D} + {}_I\mathbf{W}, \quad {}_I\mathbf{D} = \frac{1}{2}({}_I\mathbf{L} + {}_I\mathbf{L}^{\mathrm{T}}) = {}_I\mathbf{D}^{\mathrm{T}},\\
&{}_I\mathbf{W} = \frac{1}{2}({}_I\mathbf{L} - {}_I\mathbf{L}^{\mathrm{T}}) = -{}_I\mathbf{W}^{\mathrm{T}}.
\end{aligned}
\tag{12}
$$

It was shown in Refs. [1,13] that a simple form for viscous material dissipation can be developed by additively separating the constitutive equations for $\{{}_I\mathbf{T}, {}_I\mathbf{t}^i\}$ into purely elastic parts $\{{}_I\hat{\mathbf{T}}, {}_I\hat{\mathbf{t}}^i\}$ and viscous parts $\{{}_I\check{\mathbf{T}}, {}_I\check{\mathbf{t}}^i\}$, such that

$$
{}_I\mathbf{T} = {}_I\hat{\mathbf{T}} + {}_I\check{\mathbf{T}}, \quad {}_I\mathbf{t}^i = {}_I\hat{\mathbf{t}}^i + {}_I\check{\mathbf{t}}^i \quad \text{for } i = 1,2,\ldots,5.
\tag{13}
$$

In particular, the rate of material dissipation ${}_I\mathscr{D}$ is defined by

$$
{}_Id^{1/2}\,{}_I\mathscr{D} = {}_Id^{1/2}\,{}_I\mathbf{T} \cdot {}_I\mathbf{D} + ({}_I\mathbf{F}^{\mathrm{T}}\,{}_I\mathbf{t}^4) \cdot {}_I\dot{\boldsymbol{\beta}}_1 + ({}_I\mathbf{F}^{\mathrm{T}}\,{}_I\mathbf{t}^5) \cdot {}_I\dot{\boldsymbol{\beta}}_2 - {}_Im_I\dot{\Sigma} \geqslant 0,
\tag{14}
$$

where ${}_I\Sigma$ is the strain energy per unit mass. Moreover, the mechanical power of the elastic parts $\{{}_I\hat{\mathbf{T}}, {}_I\hat{\mathbf{t}}^i\}$ is balanced by the rate of change of strain energy

$$
{}_Id^{1/2}\,{}_I\hat{\mathbf{T}} \cdot {}_I\mathbf{D} + ({}_I\mathbf{F}^{\mathrm{T}}\,{}_I\hat{\mathbf{t}}^4) \cdot {}_I\dot{\boldsymbol{\beta}}_1 + ({}_I\mathbf{F}^{\mathrm{T}}\,{}_I\hat{\mathbf{t}}^5) \cdot {}_I\dot{\boldsymbol{\beta}}_2 = {}_Im_I\dot{\Sigma},
\tag{15}
$$

so that the rate of material dissipation requires the viscous terms to be dissipative

$$
{}_Id^{1/2}\,{}_I\mathscr{D} = {}_Id^{1/2}\,{}_I\check{\mathbf{T}} \cdot {}_I\mathbf{D} + ({}_I\mathbf{F}^{\mathrm{T}}\,{}_I\check{\mathbf{t}}^4) \cdot {}_I\dot{\boldsymbol{\beta}}_1 + ({}_I\mathbf{F}^{\mathrm{T}}\,{}_I\check{\mathbf{t}}^5) \cdot {}_I\dot{\boldsymbol{\beta}}_2 \geqslant 0.
\tag{16}
$$

Here, attention is confined to a homogeneous uniform material with constant three-dimensional mass density ρ_0^* in the reference configuration so that the mass ${}_Im$ of the Ith element can be written in the form

$$
{}_Im = \rho_0^*\,{}_ID^{1/2}\,{}_IV,
\tag{17}
$$

where ${}_IV$ is a volume term that will be defined later. Next, using the work of Flory [17] it is convenient to define pure measures of distortional deformation ${}_I\mathbf{F}'$, ${}_I\mathbf{C}'$ and ${}_I\mathbf{B}'$ as unimodular tensors

$$
{}_I\mathbf{F}' = {}_IJ^{-1/3}\,{}_I\mathbf{F}, \quad \det({}_I\mathbf{F}') = 1, \quad {}_I\mathbf{C}' = {}_I\mathbf{F}'^{\mathrm{T}}\,{}_I\mathbf{F}', \quad \det({}_I\mathbf{C}') = 1, \quad {}_I\mathbf{B}' = {}_I\mathbf{F}'\,{}_I\mathbf{F}'^{\mathrm{T}}, \quad \det({}_I\mathbf{B}') = 1.
\tag{18}
$$

Also, the modifications introduced by Nadler and Rubin [16] propose inhomogeneous strain measures in the forms

$$
\begin{aligned}
&{}_I\kappa_1^1 = {}_IL\,{}_I\boldsymbol{\beta}_1 \cdot {}_I\mathbf{D}^1, \quad {}_I\kappa_1^2 = {}_IW\,{}_I\boldsymbol{\beta}_1 \cdot {}_I\mathbf{D}^2, \quad {}_I\kappa_1^3 = {}_IH\,{}_I\boldsymbol{\beta}_1 \cdot {}_I\mathbf{D}^3,\\
&{}_I\kappa_2^1 = {}_IH\,{}_I\boldsymbol{\beta}_2 \cdot {}_I\mathbf{D}^1, \quad {}_I\kappa_2^2 = {}_IL\,{}_I\boldsymbol{\beta}_2 \cdot {}_I\mathbf{D}^2, \quad {}_I\kappa_2^3 = {}_IW\,{}_I\boldsymbol{\beta}_2 \cdot {}_I\mathbf{D}^3.
\end{aligned}
\tag{19}
$$

Then, a simple neo-Hookean model for isotropic nonlinear elasticity can be characterized by the strain energy function

$$
{}_I\Sigma = \Sigma^*({}_IJ, {}_I\mathbf{C}') + {}_I\Psi({}_I\boldsymbol{\beta}_\alpha),
\tag{20}
$$

where the strain energy Σ^* of the three-dimensional material characterizes homogeneous deformation and is given by

$$
2\rho_0^*\Sigma^*({}_I\mathbf{C}) = 2K^*[{}_IJ - 1 - \ln({}_IJ)] + \mu^*({}_I\mathbf{C}' \cdot \mathbf{I} - 3).
\tag{21}
$$

In this equation, K^* and μ^* are the small deformation bulk modulus and shear modulus of the three-dimensional material, respectively. Also, the strain energy ${}_I\Psi$, which characterizes inhomogeneous deformations of bending and torsion of the element, is given by

$$\begin{aligned}2{}_Im_I\Psi = {}_ID^{1/2}\,{}_IV[{}_IK_1({}_I\kappa_1^3)^2 + {}_IK_2({}_I\kappa_2^3)^2 + {}_IK_3({}_I\kappa_1^1)^2 + 2{}_IK_4({}_I\kappa_1^1\,{}_I\kappa_2^2)\\ + {}_IK_5({}_I\kappa_2^2)^2 + {}_IK_6({}_I\kappa_1^2)^2 + 2{}_IK_7({}_I\kappa_1^2\,{}_I\kappa_2^1) + {}_IK_8({}_I\kappa_2^1)^2],\end{aligned} \tag{22}$$

where ${}_IK_i$ $(i=1,2,\ldots,8)$ are constitutive constants. In Ref. [16], these constants were determined by comparison with exact solutions of bending and torsion of a rectangular parallelepiped to obtain

$$\begin{aligned}&{}_IK_1 = {}_IK_2 = \frac{E^*}{12},\quad {}_IK_3 = {}_IK_5 = \frac{E^*}{12(I-v^{*2})},\quad {}_IK_4 = \frac{v^*E^*}{12(I-v^{*2})},\\ &{}_IK_6 = \frac{{}_IH}{{}_IW}\left[\frac{\mu^*b^*({}_I\xi_3)}{6(2-{}_IK)}\right],\quad {}_IK_7 = \left[\frac{\mu^*b^*({}_I\xi_3)({}_IK-1)}{6(2-{}_IK)}\right],\quad K_8 = \frac{{}_IW}{{}_IH}\left[\frac{\mu^*b^*({}_I\xi_3)}{6(2-{}_IK)}\right],\\ &{}_IK = \mathrm{Min}\left[2-\varepsilon, \frac{1}{b^*({}_I\xi_3)}\sqrt{\frac{{}_IL^2b^*({}_I\xi_1)b^*({}_I\xi_2)}{{}_IH\,{}_IW}}\right],\quad \varepsilon = 0.1,\\ &{}_I\xi_1 = \mathrm{Max}\left\{\frac{{}_IW}{{}_IL}, \frac{{}_IL}{{}_IW}\right\},\quad {}_I\xi_2 = \mathrm{Max}\left\{\frac{{}_IH}{{}_IL}, \frac{{}_IL}{{}_IH}\right\},\quad {}_I\xi_3 = \mathrm{Max}\left\{\frac{{}_IH}{{}_IW}, \frac{{}_IW}{{}_IH}\right\},\\ &b^*(\xi) = \frac{1}{\xi}\left[1 - \frac{192}{\pi^5\xi}\sum_{n=1}^{\infty}\left[\frac{1}{(2n-1)^5}\right]\tanh\left\{\frac{\pi(2n-1)\xi}{2}\right\}\right],\end{aligned} \tag{23}$$

where E^* is Young's modulus, which is related to K^* and μ^* and Poisson's ratio v^* by

$$K^* = \frac{2\mu^*(1+v^*)}{3(1-2v^*)},\quad E^* = 2\mu^*(1+v^*). \tag{24}$$

Next, using standard arguments it can be shown that the condition Eq. (15) requires the elastic parts $\{{}_I\hat{\mathbf{T}}, {}_I\hat{\mathbf{t}}^i\}$ to be related to derivatives of the strain energy function by the expressions

$$\begin{aligned}&{}_Id^{1/2}\,{}_I\hat{\mathbf{T}} = 2{}_Im_I\mathbf{F}\frac{\partial\Sigma^*({}_I\mathbf{C})}{\partial\,{}_I\mathbf{C}}{}_I\mathbf{F}^{\mathrm{T}},\quad {}_I\hat{\mathbf{t}}^4 = {}_Im_I\mathbf{F}^{-\mathrm{T}}\frac{\partial_I\Psi}{\partial_I\boldsymbol{\beta}_1},\quad {}_I\hat{\mathbf{t}}^5 = {}_Im_I\mathbf{F}^{-\mathrm{T}}\frac{\partial_I\Psi}{\partial_I\boldsymbol{\beta}_2},\\ &{}_Id^{1/2}\,{}_I\hat{\mathbf{T}} = {}_ID^{1/2}\,{}_IVK^*[{}_IJ-1]\mathbf{I} + {}_ID^{1/2}\,{}_IV\mu^*\left[{}_I\mathbf{B}' - \frac{1}{3}({}_I\mathbf{B}'\cdot\mathbf{I})\mathbf{I}\right],\\ &{}_I\hat{\mathbf{t}}^4 = {}_ID^{1/2}\,{}_IV[{}_IL\{{}_IK_3\,{}_I\kappa_1^1 + {}_IK_4\,{}_I\kappa_2^2\}{}_I\mathbf{d}^1 + {}_IW\{{}_IK_6\,{}_I\kappa_1^2 + {}_IK_7\,{}_I\kappa_2^1\}{}_I\mathbf{d}^2 + {}_IH\{{}_IK_1\,{}_I\kappa_1^3\}{}_I\mathbf{d}^3],\\ &{}_I\hat{\mathbf{t}}^5 = {}_ID^{1/2}\,{}_IV[{}_IH\{{}_IK_7\,{}_I\kappa_1^2 + {}_IK_8\,{}_I\kappa_2^1\}{}_I\mathbf{d}^1 + {}_IL\{{}_IK_4\,{}_I\kappa_1^1 + {}_IK_5\,{}_I\kappa_2^2\}{}_I\mathbf{d}^2 + {}_IW\{{}_IK_2\,{}_I\kappa_2^3\}{}_I\mathbf{d}^3],\\ &{}_I\hat{\mathbf{t}}^i = [{}_Id^{1/2}\,{}_I\hat{\mathbf{T}} - {}_I\hat{\mathbf{t}}^4\otimes{}_I\mathbf{d}_4 - {}_I\hat{\mathbf{t}}^5\otimes{}_I\mathbf{d}_5]\cdot{}_I\mathbf{d}^i\quad\text{for } i=1,2,3.\end{aligned} \tag{25}$$

The constitutive equations proposed in Ref. [11] for the viscous parts $\{{}_I\check{\mathbf{T}}, {}_I\check{\mathbf{t}}^i\}$ do not allow independent control of damping due to torsion, and bending in the two principal directions. Therefore, to remove this deficiency those constitutive equations are generalized to take the forms

$$\begin{aligned}&{}_Id^{1/2}\,{}_I\check{\mathbf{T}} = {}_ID^{1/2}\,{}_IV[{}_I\eta_1({}_I\mathbf{D}\cdot\mathbf{I})\mathbf{I} + 2{}_I\eta_2\mathbf{D}'],\\ &{}_I\check{\mathbf{t}}^4 = {}_ID^{1/2}\,{}_IV({}_I\mathbf{D}^1\cdot{}_I\mathbf{D}^1){}_I\mathbf{F}^{-\mathrm{T}}[\tfrac{1}{2}{}_I\eta_3({}_I\mathbf{D}_2\cdot{}_I\mathbf{D}_2)({}_I\mathbf{D}^2\cdot{}_I\dot{\boldsymbol{\beta}}_1){}_I\mathbf{D}^2\\ &\qquad + {}_I\eta_4({}_I\mathbf{D}_3\cdot{}_I\mathbf{D}_3)({}_I\mathbf{D}^3\cdot{}_I\dot{\boldsymbol{\beta}}_1){}_I\mathbf{D}^3],\\ &{}_I\check{\mathbf{t}}^5 = {}_ID^{1/2}\,{}_IV({}_I\mathbf{D}^2\cdot{}_I\mathbf{D}^2){}_I\mathbf{F}^{-\mathrm{T}}[\tfrac{1}{2}{}_I\eta_3({}_I\mathbf{D}_1\cdot{}_I\mathbf{D}_1)({}_I\mathbf{D}^1\cdot{}_I\dot{\boldsymbol{\beta}}_2){}_I\mathbf{D}^1\\ &\qquad + {}_I\eta_5({}_I\mathbf{D}_3\cdot{}_I\mathbf{D}_3)({}_I\mathbf{D}^3\cdot{}_I\dot{\boldsymbol{\beta}}_2){}_I\mathbf{D}^3],\\ &{}_I\check{\mathbf{t}}^i = [{}_Id^{1/2}\,{}_I\check{\mathbf{T}} - {}_I\check{\mathbf{t}}^4\otimes{}_I\mathbf{d}_4 - {}_I\check{\mathbf{t}}^5\otimes{}_I\mathbf{d}_5]\cdot{}_I\mathbf{d}^i\quad\text{for } i=1,2,3,\end{aligned} \tag{26}$$

where ${}_I\mathbf{D}'$ is the deviatoric part of ${}_I\mathbf{D}$:

$$ {}_I\mathbf{D}' = {}_I\mathbf{D} - \tfrac{1}{3}({}_I\mathbf{D}\cdot\mathbf{I})\mathbf{I}. \tag{27} $$

Then, substituting Eq. (26) into Eq. (16) indicates that the rate of material dissipation will be non-negative if the viscosity coefficients ${}_I\eta_i$ are non-negative. Also, it is noted that the constants $\{{}_I\eta_1, {}_I\eta_2, {}_I\eta_3, {}_I\eta_4, {}_I\eta_5\}$ control the viscosity to: dilatation, distortion, torsion, and bending in two orthogonal planes, respectively.

Dissipation to aerodynamic drag can also be included. Specifically, for a constant body force $\mathbf{b}^*$ per unit mass, and in the absence of tractions on the lateral surface of the Ith element, the assigned fields ${}_I\mathbf{B}^i$ in Eq. (8) are specified by

$$ \begin{aligned} &{}_Im_I\mathbf{B}^0 = {}_Im\mathbf{b}^* - {}_IC_D\rho_A|{}_I\mathbf{w}_0|{}_I\mathbf{w}_0, \quad {}_IC_D = 0 \quad \text{for } I = 1,2,\ldots,N-1, {}_NC_D = C_D,\\ &A = BH, \quad {}_Im_I\mathbf{B}_i = {}_Im_I y^{0i}\mathbf{b}^* \quad \text{for } i = 1,2,\ldots,5, \end{aligned} \tag{28} $$

where C_D is the drag coefficient, ρ_a the density of air, A the effective area of the element, ${}_I\mathbf{w}_0$ the velocity of the element's centroid relative to the velocity of the air, which is assumed to be zero. Also, in the following simulations aerodynamic drag is added only to the last element $I = N$, which represents the mass attached to the beam.

For the numerical solution procedure, it is convenient to use the relations [12]

$$ \mathbf{m}_1^3 = -\frac{{}_IL}{2}\mathbf{m}_1^0, \quad \mathbf{m}_2^3 = \frac{{}_IL}{2}\mathbf{m}_2^0, \quad \mathbf{m}_1^4 = -\frac{{}_IL}{2}\mathbf{m}_1^1, \quad \mathbf{m}_2^4 = \frac{{}_IL}{2}\mathbf{m}_2^1, \quad \mathbf{m}_1^5 = -\frac{{}_IL}{2}\mathbf{m}_1^2, \quad \mathbf{m}_2^5 = \frac{{}_IL}{2}\mathbf{m}_2^2 \tag{29} $$

to reformulate the equations of motion (7) in the alternative forms

$$ \begin{aligned} {}_I\mathbf{m}_1^0 &= \frac{1}{{}_IL}\left[\frac{{}_IL}{2}\left\{{}_Im_I y^{00}\,{}_I\dot{\mathbf{w}}_0 - {}_Im_I\mathbf{B}^0\right\} - \left\{{}_Im_I y^{33}\,{}_I\dot{\mathbf{w}}_3 - {}_Im_I\mathbf{B}^3 + {}_I\mathbf{t}^3\right\}\right],\\ {}_I\mathbf{m}_2^0 &= \frac{1}{{}_IL}\left[\frac{{}_IL}{2}\left\{{}_Im_I y^{00}\,{}_I\dot{\mathbf{w}}_0 - {}_Im_I\mathbf{B}^0\right\} + \left\{{}_Im_I y^{33}\,{}_I\dot{\mathbf{w}}_3 - {}_Im_I\mathbf{B}^3 + {}_I\mathbf{t}^3\right\}\right],\\ {}_I\mathbf{m}_1^1 &= \frac{1}{{}_IL}\left[\frac{{}_IL}{2}\left\{{}_Im_I y^{11}\,{}_I\dot{\mathbf{w}}_1 - {}_Im_I\mathbf{B}^1 + {}_I\mathbf{t}^1\right\} - \left\{{}_Im_I y^{44}\,{}_I\dot{\mathbf{w}}_4 - {}_Im_I\mathbf{B}^4 + {}_I\mathbf{t}^4\right\}\right],\\ {}_I\mathbf{m}_2^1 &= \frac{1}{{}_IL}\left[\frac{{}_IL}{2}\left\{{}_Im_I y^{11}\,{}_I\dot{\mathbf{w}}_1 - {}_Im_I\mathbf{B}^1 + {}_I\mathbf{t}^1\right\} + \left\{{}_Im_I y^{44}\,{}_I\dot{\mathbf{w}}_4 - {}_Im_I\mathbf{B}^4 + {}_I\mathbf{t}^4\right\}\right],\\ {}_I\mathbf{m}_1^2 &= \frac{1}{{}_IL}\left[\frac{{}_IL}{2}\left\{{}_Im_I y^{22}\,{}_I\dot{\mathbf{w}}_2 - {}_Im_I\mathbf{B}^2 + {}_I\mathbf{t}^2\right\} - \left\{{}_Im_I y^{55}\,{}_I\dot{\mathbf{w}}_5 - {}_Im_I\mathbf{B}^5 + {}_I\mathbf{t}^5\right\}\right],\\ {}_I\mathbf{m}_2^2 &= \frac{1}{{}_IL}\left[\frac{{}_IL}{2}\left\{{}_Im_I y^{22}\,{}_I\dot{\mathbf{w}}_2 - {}_Im_I\mathbf{B}^2 + {}_I\mathbf{t}^2\right\} + \left\{{}_Im_I y^{55}\,{}_I\dot{\mathbf{w}}_5 - {}_Im_I\mathbf{B}^5 + {}_I\mathbf{t}^5\right\}\right], \end{aligned} \tag{30} $$

which have been specialized for the case where the off-diagonal terms of ${}_Iy^{ij}$ vanish. Kinematic coupling of the elements has already been considered by Eq. (2), which connect the element directors ${}_I\mathbf{d}_i$ to the nodal directors ${}_I\mathbf{d}_i^*$. Additional kinetic coupling equations associated with the interior nodes require [11,12]

$$ {}_{I-1}\mathbf{m}_2^i + {}_I\mathbf{m}_1^i = 0 \quad \text{for } I = 2,3,\ldots,N \quad \text{and} \quad i = 0,1,2. \tag{31} $$

Also, the boundary conditions are characterized by specifying

$$ \begin{aligned} &\{{}_1\mathbf{d}_0^* \text{ or } {}_1\mathbf{m}_1^0\} \quad \text{and} \quad \{{}_1\mathbf{d}_1^* \text{ or } {}_1\mathbf{m}_1^1\} \quad \text{and} \quad \{{}_1\mathbf{d}_2^* \text{ or } {}_1\mathbf{m}_1^2\},\\ &\{{}_{N+1}\mathbf{d}_0^* \text{ or } {}_N\mathbf{m}_2^0\} \quad \text{and} \quad \{{}_{N+1}\mathbf{d}_1^* \text{ or } {}_N\mathbf{m}_2^1\} \quad \text{and} \quad \{{}_{N+1}\mathbf{d}_2^* \text{ or } {}_N\mathbf{m}_2^2\}. \end{aligned} \tag{32} $$

Thus, with the help of the kinematic conditions (2), (11), (12), (18), (19), the constitutive equations (13), (25), (26), and the results (30), the coupling Eq. (31) and the boundary conditions (32) yield a system of $3(N+1)$ ordinary differential equations for the $3(N+1)$ nodal directors ${}_I\mathbf{d}_i^*$ ($I = 1,2,\ldots,N+1$; $i = 0,1,2$), which require specification of initial conditions for the quantities

$$ \{{}_I\mathbf{d}_i^*(0),\ {}_I\mathbf{w}_i^*(0)\} \quad \text{for} \quad I = 1,2,\ldots,N+1 \quad \text{and} \quad i = 0,1,2. \tag{33} $$

For later reference it is noted that the kinetic energy ${}_I\mathscr{K}$ of the Ith element is given by

$$ {}_I\mathscr{K} = \tfrac{1}{2}\,{}_I m[{}_I\mathbf{w}_0 \cdot {}_I\mathbf{w}_0 + {}_I y^{11}\,{}_I\mathbf{w}_1 \cdot {}_I\mathbf{w}_1 + {}_I y^{22}\,{}_I\mathbf{w}_2 \cdot {}_I\mathbf{w}_2 + {}_I y^{33}\,{}_I\mathbf{w}_3 \cdot {}_I\mathbf{w}_3 + {}_I y^{44}\,{}_I\mathbf{w}_4 \cdot {}_I\mathbf{w}_4 + {}_I y^{55}\,{}_I\mathbf{w}_5 \cdot {}_I\mathbf{w}_5], \tag{34} $$

so that the total kinetic energy $\mathscr{K}$ and total strain energy $\mathscr{U}$ of the beam–mass system are given by

$$ \mathscr{K} = \sum_{I=1}^{N} {}_I\mathscr{K}, \quad \mathscr{U} = \sum_{I=1}^{N} {}_I m_I \Sigma. \tag{35} $$

Also, from Ref. [13] it can be shown that the mechanical moment ${}_{I+1}\mathbf{m}$ applied to the cross-section $I+1$ of the Ith element about its centroid is given by

$$ {}_{I+1}\mathbf{m} = {}_{I+1}\mathbf{d}_1^* \times {}_I\mathbf{m}_2^1 + {}_{I+1}\mathbf{d}_2^* \times {}_I\mathbf{m}_2^2 \quad \text{for } I = 1, 2, \ldots, N. \tag{36} $$

Moreover, using Eq. (30) it follows that the viscous part ${}_{I+1}\check{\mathbf{m}}$ of the mechanical moment ${}_{I+1}\mathbf{m}$ applied to the cross-section $I+1$ of the Ith element is given by

$$ {}_{I+1}\check{\mathbf{m}} = {}_{I+1}\mathbf{d}_1^* \times \left[\frac{1}{2}{}_I\check{\mathbf{t}}^1 + \frac{1}{{}_I L}{}_I\check{\mathbf{t}}^4\right] + {}_{I+1}\mathbf{d}_2^* \times \left[\frac{1}{2}{}_I\check{\mathbf{t}}^2 + \frac{1}{{}_I L}{}_I\check{\mathbf{t}}^5\right]. \tag{37} $$

3. Problem formulation

For simplicity, instead of modeling the mass as a rigid body it is modeled as another Cosserat point with different dimensions from those associated with the beam. Also, in Ref. [1] it was noted that the flexibility of the extension bar attached to the motor shaft and the bearings holding this extension bar in the experimental setup all contribute to damping of the system, which is difficult to model explicitly. Therefore, here a small element of length c was introduced at the beam's clamped end to simulate damping of the experimental system. Specifically, the beam–mass system is modeled by N Cosserat points with the beam being divided into $M = N-2$ equal elements. Consequently, the dimensions of the elements are given by

$$ \begin{aligned} &{}_1H = h, \;\; {}_1W = w, \;\; {}_1L = c, \\ &{}_I H = h, \;\; {}_I W = w, \;\; {}_I L = \frac{L-c}{M} \quad \text{for } I = 2, 3, \ldots, M = N-1, \\ &{}_N H = H, \;\; {}_N W = W, \;\; {}_N L = B. \end{aligned} \tag{38} $$

Moreover, the reference values of the nodal directors are given by

$$ \begin{aligned} &{}_1\mathbf{D}_0^* = R\mathbf{e}_3, \;\; {}_1\mathbf{D}_0^* = \left[R + c + (I-2)\frac{(L-c)}{M}\right]\mathbf{e}_3 \quad \text{for } I = 2, 3, \ldots, M+2 = N, \\ &{}_{N+1}\mathbf{D}_0^* = (R + L + B)\mathbf{e}_3, \;\; {}_I\mathbf{D}_1^* = \mathbf{e}_1, \;\; {}_1\mathbf{D}_2^* = \mathbf{e}_2 \quad \text{for } I = 1, 2, \ldots, N+1, \end{aligned} \tag{39} $$

so that the reference element directors ${}_I\mathbf{D}_i$ and the reciprocal directors ${}_I\mathbf{D}^i$ are given by

$$ \begin{aligned} &{}_1\mathbf{D}_0 = \left[R + \frac{c}{2}\right]\mathbf{e}_3, \;\; {}_1\mathbf{D}_0 = \left[R + c + \left(I - \frac{3}{2}\right)\frac{(L-c)}{M}\right]\mathbf{e}_3 \quad \text{for } I = 2, 3, \ldots, M+1 = N-1, \\ &{}_N\mathbf{D}_0 = \left(R + L + \frac{B}{2}\right)\mathbf{e}_3, \;\; {}_I\mathbf{D}_i = {}_I\mathbf{D}^i = \mathbf{e}_i \quad \text{for } i = 1, 2, 3 \text{ and } I = 1, 2, \ldots, N, \\ &{}_I\mathbf{D}_4 = {}_I\mathbf{D}_5 = 0 \quad \text{for } I = 2, 3, \ldots, N. \end{aligned} \tag{40} $$

Moreover, it can be shown [11,12] that for the beam elements

$$ \begin{aligned} &{}_I D^{1/2} = 1, \;\; {}_I V = {}_I H\,{}_I W\,{}_I L, \;\; {}_I y^{00} = 1, \;\; {}_I y^{11} = \frac{{}_I H^2}{\pi^2}, \;\; {}_I y^{22} = \frac{{}_I W^2}{\pi^2}, \;\; {}_I y^{33} = \frac{{}_I L^2}{\pi^2}, \;\; {}_I y^{44} = {}_I y^{55} = \left[\frac{2\,{}_I L}{3\pi}\right]^4, \\ &\text{all other } {}_I y^{ij} = 0 \quad \text{for } I = 1, 2, \ldots, M+1, \end{aligned} \tag{41} $$

where a typographical error in the expressions for ${}_I y^{44}$ and ${}_I y^{55}$ has been corrected. The director inertia coefficients for the beam elements model the distribution of inertia in shearing and extensional modes of

deformation. However, for the mass attached to the beam's end these director inertia coefficients are specified by values consistent with a rigid body so that

$$
{}_N D^{1/2} = 1, \quad {}_N V = {}_N H_N W_N L, \quad {}_N y^{00} = 1, \quad {}_N y^{11} = \frac{{}_N H^2}{12}, \quad {}_N y^{22} = \frac{{}_N W^2}{12}, \quad {}_N y^{33} = \frac{{}_N L^2}{12},
$$
$$
{}_N y^{44} = {}_N y^{55} = \left[\frac{2_N L}{3\sqrt{12}}\right]^4 \quad \text{all other } {}_N y^{ij} = 0. \tag{42}
$$

In general, the motion of the beam–mass system is fully three-dimensional so that the nodal director vectors ${}_I\mathbf{d}_i^*$ are general vector functions of time to be determined. The boundary conditions at the clamped end of the beam require

$$
{}_I\mathbf{d}_0^* = R(\sin\,\phi\mathbf{e}_1 + \cos\,\phi\mathbf{e}_3), \;\; {}_I\mathbf{d}_1^* = \cos\,\phi\mathbf{e}_1 - \sin\,\phi\mathbf{e}_3, \;\; {}_I\mathbf{d}_2^* = \mathbf{e}_2, \tag{43}
$$

where ϕ is given by Eq. (1). Also, the end of the mass is taken to be free of tractions so that the remaining boundary conditions require

$$
{}_N\mathbf{m}_2^i = 0 \quad \text{for } i = 0, 1, 2. \tag{44}
$$

To complete the formulation it is noted that the material constants $\{E^*, v^*\}$ are given by the values $\{E, v\}$ in Table 1 of Ref. [1], and the geometric parameters $\{R, h, w, L, H, W, B\}$ are given by the values in that table. Moreover, the reference density ρ_0^* is given by the values of ρ_{avg} in that table for the beam elements and the mass element. Also, the body force is given by

$$
\mathbf{b}^* = \alpha g\mathbf{e}_3, \tag{45}
$$

where g ($= 9.81\,\text{m/s}^2$) is the force of gravity per unit mass, $\alpha = -1$ indicates that the mass is directly above the beam's clamped end, and $\alpha = 1$ indicates that the mass is directly below the beam's clamped end. Furthermore, the length c of the element modeling the clamping system is specified by

$$
c = 1\,\text{mm}. \tag{46}
$$

4. Newmark implicit integration

It is well known that explicit time integration of the nonlinear equations for rods can be quite time consuming [9]. Consequently, some form of implicit integration is usually employed. Here, the Newmark scheme is used to express the nodal director velocities ${}_I\mathbf{w}_i^*(t_{n+I})$ and accelerations ${}_I\dot{\mathbf{w}}_i^*(t_{n+I})$ at the end $t = t_{n+1}$ of a time step $\Delta t = t_{n+1} - t_n$, in terms of the quantities $\{{}_I\mathbf{d}_i^*(t_n),\;\; {}_I\mathbf{w}_i^*(t_n),\;\; {}_I\dot{\mathbf{w}}_i^*(t_n)\}$ at the beginning $t = t_n$ of the time step and the values ${}_I\mathbf{d}_i^*(t_{n+1})$ of the nodal directors at the end of the time step. Specifically, the Newmark scheme is specified in the form

$$
\begin{aligned}
&{}_I\dot{\mathbf{w}}_i^*(t_{n+1}) = a_3[{}_I\mathbf{d}_i^*(t_{n+1}) - {}_I\mathbf{d}_i^*(t_n)] - a_4[{}_I\mathbf{w}_i^*(t_n)] - a_5[{}_I\dot{\mathbf{w}}_i^*(t_n)] \quad \text{for } i = 0, 1, 2,\\
&{}_I\dot{\mathbf{w}}_i^*(t_{n+1}) = {}_I\mathbf{w}_i^*(t_n) + a_2[{}_I\dot{\mathbf{w}}_i^*(t_n)] + a_1[{}_I\dot{\mathbf{w}}_i^*(t_{n+1})] \quad \text{for } i = 0, 1, 2,\\
&\qquad a_1 = \gamma\,\Delta t, \;\; a_2 = (1-\gamma)\,\Delta t, \;\; a_3 = \frac{1}{\beta(\Delta t)^2}, \;\; a_4 = \frac{1}{\beta\,\Delta t}, \;\; a_5\frac{1-2\beta}{2\beta},
\end{aligned} \tag{47}
$$

where the auxiliary constants a_i have been introduced for convenience and the constants $\{\gamma, \beta\}$ are specified by the typical values

$$
\gamma = \tfrac{1}{2}, \quad \beta = \tfrac{1}{4}. \tag{48}
$$

Using expressions (47), the coupling equation (31) and the boundary conditions (43) and (44) yield a system of $3(N+1)$ algebraic vector equations, which can be expressed in the forms

$$
{}_J\mathbf{f}^j\left({}_I\mathbf{d}_i^*(t_{n+1})\right) = 0 \quad \text{for } I; J = 1, 2, \ldots, N+1 \text{ and } i, j = 0, 1, 2 \tag{49}
$$

for each time step, where the functions ${}_I\mathbf{f}^i$ are specified by

$$
\begin{aligned}
&{}_1\mathbf{f}^0 = {}_1\mathbf{d}_0^* - R(\sin\phi\mathbf{e}_1 + \cos\phi\mathbf{e}_3), \quad {}_1\mathbf{f}^1 = {}_1\mathbf{d}_1^* - (\cos\phi\mathbf{e}_1 - \sin\phi\mathbf{e}_3), \quad {}_1\mathbf{f}^2 = {}_1\mathbf{d}_2^* - \mathbf{e}_2,\\
&{}_1\mathbf{f}^i = {}_{I-1}\mathbf{m}_2^i + {}_I\mathbf{m}_1^i = 0 \quad \text{for } I = 2,3,\ldots,N \text{ and } i = 0,1,2,\\
&{}_{N+1}\mathbf{f}^i = {}_N\mathbf{m}_2^i \quad \text{for } i = 0,1,2.
\end{aligned} \tag{50}
$$

Integration is started by specifying initial conditions of the form Eq. (33). The values of ${}_I\dot{\mathbf{w}}_i^*(0)$ are determined here by solving the equations of motion at $t = 0$; however, it is also common to set these values equal to zero and to correct them during the second time step. Moreover, Eq. (49) can be solved using a Newton–Raphson iteration scheme, which determines the value ${}_I\mathbf{d}_i^*(t_{n+1})_{K+1}$ associated with the Kth iteration by solving the equations

$$
\begin{aligned}
&0 = {}_I\mathbf{f}^i({}_I\mathbf{d}_i^*(t_{n+1})_K) + \Delta({}_I\mathbf{f}^i), \quad \Delta({}_I\mathbf{d}_i^*) = {}_I\mathbf{d}_i^*(t_{n+1})_{K+1} - {}_I\mathbf{d}_i^*(t_{n+1})_K\\
&\quad \text{for } I = 1,2,\ldots N+1 \text{ and } i = 0,1,2,\\
&\Delta({}_1\mathbf{f}^i) = \sum_{j=0}^{2}[{}_1\mathbf{B}^{ij}\cdot\Delta({}_1\mathbf{d}_j^*) + {}_1\mathbf{C}^{ij}\cdot\Delta({}_2\mathbf{d}_j^*)] \quad \text{for } i = 0,1,2,\\
&\Delta({}_1\mathbf{f}^i) = \sum_{j=0}^{2}[{}_1\mathbf{A}^{ij}\cdot\Delta({}_{I-1}\mathbf{d}_j^*) + {}_1\mathbf{B}^{ij}\cdot\Delta({}_I\mathbf{d}_j^*) + {}_I\mathbf{C}^{ij}\cdot\Delta({}_{I+1}\mathbf{d}_j^*)]\\
&\quad \text{for } I = 2,3,\ldots,N \text{ and } i = 0,1,2,\\
&\Delta({}_{N+1}\mathbf{f}^i) = \sum_{j=0}^{2}[{}_{N+1}\mathbf{A}^{ij}\cdot\Delta({}_N\mathbf{d}_j^*) + {}_{N+1}\mathbf{B}^{ij}\cdot\Delta({}_{N+1}\mathbf{d}_j^*)] \quad \text{for } i = 0,1,2,
\end{aligned} \tag{51}
$$

where the second-order tensors $\{{}_I\mathbf{A}^{ij},\ {}_I\mathbf{B}^{ij},\ {}_I\mathbf{C}^{ij}\}$ $(i,j = 0,1,2)$ characterize the tangent stiffness, which is evaluated at the Kth iteration ${}_I\mathbf{d}_i^*(t_{n+1})_K$. The solution of $\Delta({}_I\mathbf{d}_i^*)$ is used to determine the updated guess ${}_I\mathbf{d}_i^*(t_{n+1})_{K+1}$ for ${}_I\mathbf{d}_i^*$ at the end of the time step. Also, the first guess in the iteration procedure can be specified by

$$
{}_I\mathbf{d}_i^*(t_{n+1})_K = {}_I\mathbf{d}_i^*(t_n) \quad \text{for } K = 1 \text{ and } i = 0,1,2 \tag{52}
$$

and the iteration converges when the maximum residual R_K

$$
R_K = \mathrm{Max}|{}_J\mathbf{f}^j({}_I\mathbf{d}_i^*(t_{n+1})_K)| \quad \text{for all } J,j,I,i \tag{53}
$$

satisfies a specified convergence criterion.

In order to determine an analytical expression for the tensors $\{{}_I\mathbf{A}^{ij},\ {}_I\mathbf{B}^{ij},\ {}_I\mathbf{C}^{ij}\}$ $(i,j = 0,1,2)$ it is convenient to develop auxiliary expressions in terms of changes $\Delta({}_I\mathbf{d}_i)$ in the element directors such that

$$
\begin{aligned}
&\Delta({}_I\mathbf{t}^i) = \sum_{j=1}^{5}{}_I\mathbf{K}^{ij}\cdot\Delta({}_I\mathbf{d}_j), \quad \Delta({}_I\hat{\mathbf{t}}^i) = \sum_{j=1}^{5}{}_I\hat{\mathbf{K}}^{ij}\cdot\Delta({}_I\mathbf{d}_j), \quad \Delta({}_I\check{\mathbf{t}}^i) = \sum_{j=1}^{5}{}_I\check{\mathbf{K}}^{ij}\cdot\Delta({}_I\mathbf{d}_j),\\
&{}_I\mathbf{K}^{ij} = {}_I\hat{\mathbf{K}}^{ij} + {}_I\check{\mathbf{K}}^{ij} \quad \text{for } I = 1,2,\ldots,N \text{ and } i,j = 1,2,\ldots,5,\\
&\Delta({}_Im_I\mathbf{B}^0) = \sum_{j=0}^{5}{}_I\mathbf{N}^{0j}\cdot\Delta({}_I\mathbf{d}_j), \quad {}_I\mathbf{N}^{0j} = 0 \quad \text{for } I = 1,2,\ldots N-1 \text{ and } j = 0,1,\ldots,5,\\
&\Delta({}_I\mathbf{m}_\alpha^i) = \sum_{j=0}^{5}{}_I\mathbf{M}_\alpha^{ij}\cdot\Delta({}_I\mathbf{d}_j) \quad \text{for } I = 1,2,\ldots,N \text{ and } i = 0,1,2 \text{ and } \alpha = 1,2,
\end{aligned} \tag{54}
$$

where the second-order tensors $\{{}_I\hat{\boldsymbol{\tau}}^{ij}, {}_I\check{\boldsymbol{\tau}}^{ij}, {}_I\mathbf{K}^{ij}, {}_I\hat{\mathbf{K}}^{ij}, {}_I\check{\mathbf{K}}^{ij}$ for $i,j = 1,2,\ldots,5\}$, $\{{}_I\mathbf{N}^{0j}$ for $j = 0,1,\ldots,5\}$, $\{{}_I\mathbf{M}_\alpha^{ij}$ for $i = 0,1,2$ and $j = 0,1,\ldots,5\}$ are determined in Appendix A. Next, with the help of Eq. (2), $\Delta({}_I\mathbf{d}_i)$ are related to

changes $\Delta({}_I\mathbf{d}_i^*)$ in the nodal directors by the expressions

$$\Delta({}_I\mathbf{d}_i) = \frac{1}{2}[\Delta({}_I\mathbf{d}_i^*) + \Delta({}_{I+1}\mathbf{d}_i^*)],$$
$$\Delta({}_I\mathbf{d}_{3+i}) = \frac{1}{{}_IL}[-\Delta({}_I\mathbf{d}_i^*) + \Delta({}_{I+1}\mathbf{d}_i^*)] \quad i = 0,1,2, \tag{55}$$

so that

$$\Delta({}_I\mathbf{m}_\alpha^i) = \sum_{j=0}^{2}\left[\frac{1}{2}{}_I\mathbf{M}_\alpha^{ij} - \frac{1}{{}_IL}{}_I\mathbf{M}_\alpha^{i(3+j)}\right]\cdot\Delta({}_I\mathbf{d}_j^*) + \sum_{j=0}^{2}\left[\frac{1}{2}{}_I\mathbf{M}_\alpha^{ij} + \frac{1}{{}_IL}{}_I\mathbf{M}_\alpha^{i(3+j)}\right]\cdot\Delta({}_{I+1}\mathbf{d}_j^*)$$
$$\text{for } I = 1,2,\ldots,N \text{ and } i = 0,1,2 \text{ and } \alpha = 1,2. \tag{56}$$

Then, the tensors $\{{}_I\mathbf{A}^{ij},\ {}_I\mathbf{B}^{ij},\ {}_I\mathbf{C}^{ij} \text{ for } i,j = 0,1,2\}$ associated with the tangent stiffness Eq. (51) can be expressed in the forms

$${}_1\mathbf{B}^{00} = {}_1\mathbf{B}^{11} = {}_1\mathbf{B}^{22} = \frac{1}{2}\mathbf{I},\ {}_1\mathbf{B}^{01} = {}_1\mathbf{B}^{02} = {}_1\mathbf{B}^{10} = {}_1\mathbf{B}^{12} = {}_1\mathbf{B}^{20} = {}_1\mathbf{B}^{21} = 0,\ {}_1\mathbf{C}^{ij} = {}_1\mathbf{B}^{ij},$$
$${}_1\mathbf{A}^{ij} = \left[\frac{1}{2}{}_{I-1}\mathbf{M}_2^{ij} - \frac{1}{{}_{I-1}L}{}_{I-1}\mathbf{M}_2^{i(3+j)}\right],$$
$${}_1\mathbf{B}^{ij} = \left[\frac{1}{2}{}_{I-1}\mathbf{M}_2^{ij} + \frac{1}{{}_{I-1}L}{}_{I-1}\mathbf{M}_2^{i(3+j)}\right] + \left[\frac{1}{2}{}_I\mathbf{M}_1^{ij} - \frac{1}{{}_IL}{}_I\mathbf{M}_1^{i(3+j)}\right],$$
$${}_1\mathbf{C}^{ij} = \left[\frac{1}{2}{}_I\mathbf{M}_1^{ij} + \frac{1}{{}_IL}{}_I\mathbf{M}_1^{i(3+j)}\right] \quad \text{for } I = 2,3,\ldots,N \text{ and } i,j = 0,1,2,$$
$${}_{N+1}\mathbf{A}^{ij} = \left[\frac{1}{2}{}_N\mathbf{M}_2^{ij} - \frac{1}{{}_NL}{}_N\mathbf{M}_2^{i(3+j)}\right],\quad {}_{N+1}\mathbf{B}^{ij} = \left[\frac{1}{2}{}_N\mathbf{M}_2^{ij} + \frac{1}{{}_NL}{}_N\mathbf{M}_2^{i(3+j)}\right]$$
$$\text{for } i,j = 0,1,2. \tag{57}$$

5. Linarized equations of motion and calibration of the damping coefficients

In order to determine values of the viscosities ${}_I\eta_i$ in Eq. (26) it is convenient to develop the linearized forms of the equations of motion (30). To this end, the nodal director displacements ${}_I\boldsymbol{\delta}_i^*$ and the element director displacements ${}_I\boldsymbol{\delta}_i$ are introduced such that

$${}_I\mathbf{d}_i^* = {}_I\mathbf{D}_i^* + {}_I\boldsymbol{\delta}_i^*,\ {}_I\mathbf{d}_i = {}_I\mathbf{D}_i + {}_I\boldsymbol{\delta}_i,$$
$${}_I\boldsymbol{\delta}_i = \tfrac{1}{2}({}_I\boldsymbol{\delta}_i^* + {}_{I+1}\boldsymbol{\delta}_i^*),\ {}_I\boldsymbol{\delta}_{3+i} = \tfrac{1}{{}_IL}({}_{I+1}\boldsymbol{\delta}_i^* - {}_I\boldsymbol{\delta}_i^*) \quad \text{for } i = 0,1,2. \tag{58}$$

Then, neglecting quadratic terms in these director displacements, the kinematic quantities Eq. (11) for the beam–mass system can be approximated by

$${}_I\mathbf{F} = \mathbf{I} + {}_I\mathbf{H},\ {}_I\mathbf{H} = \sum_{i=1}^{3}{}_I\boldsymbol{\delta}_i \otimes \mathbf{e}_i,\ {}_I\mathbf{E} = \tfrac{1}{2}({}_I\mathbf{H} + {}_I\mathbf{H}^{\mathrm{T}}),$$
$${}_IJ = 1 + {}_I\mathbf{E}\cdot\mathbf{I},\ {}_I\mathbf{C} = {}_I\mathbf{B} = \mathbf{I} + 2{}_I\mathbf{E},\ {}_I\mathbf{C}' = {}_I\mathbf{B}' = \mathbf{I} + 2{}_I\mathbf{E}',$$
$${}_I\mathbf{E}' = {}_I\mathbf{E} - \tfrac{1}{3}({}_I\mathbf{E}\cdot\mathbf{I})\mathbf{I},\ {}_I\mathbf{D} = {}_I\dot{\mathbf{E}},\ {}_I\mathbf{D}' = {}_I\dot{\mathbf{E}}',\ {}_I\boldsymbol{\beta}_1 = {}_I\boldsymbol{\delta}_4,\ {}_I\boldsymbol{\beta}_2 = {}_I\boldsymbol{\delta}_5,$$
$${}_I\kappa_1^1 = {}_IL_I\boldsymbol{\delta}_4\cdot\mathbf{e}_1,\ {}_I\kappa_1^2 = {}_IW_I\boldsymbol{\delta}_4\cdot\mathbf{e}_2,\ {}_I\kappa_1^3 = {}_IH_I\boldsymbol{\delta}_4\cdot\mathbf{e}_3,$$
$${}_I\kappa_2^1 = {}_IH_I\boldsymbol{\delta}_5\cdot\mathbf{e}_1,\ {}_I\kappa_2^2 = {}_IL_I\boldsymbol{\delta}_5\cdot\mathbf{e}_2,\ {}_I\kappa_2^3 = {}_IW_I\boldsymbol{\delta}_5\cdot\mathbf{e}_3. \tag{59}$$

Next, with the help of Eqs. (13), (25) and (26), the constitutive equations reduce to

$$
\begin{aligned}
{}_I d^{1/2}\,{}_I\hat{\mathbf{T}} &= {}_I V[K^*({}_I\mathbf{E}\cdot\mathbf{I})\mathbf{I} + 2\mu^*\,{}_I\mathbf{E}'], \quad {}_I d^{1/2}\,{}_I\check{\mathbf{T}} = {}_I V[{}_I\eta_1({}_I\dot{\mathbf{E}}\cdot\mathbf{I})\mathbf{I} + 2{}_I\eta_2\,{}_I\dot{\mathbf{E}}'],\\
{}_I\hat{\mathbf{t}}^4 &= {}_I V[{}_I L\{{}_I K_3\,{}_I\kappa_1^1 + {}_I K_4\,{}_I\kappa_2^2\}\mathbf{e}_1 + W\{{}_I K_6\,{}_I\kappa_1^2 + {}_I K_7\,{}_I\kappa_2^1\}\mathbf{e}_2 + H\{{}_I K_1\,{}_I\kappa_1^3\}\mathbf{e}_3],\\
{}_I\hat{\mathbf{t}}^5 &= {}_I V[H\{{}_I K_7\,{}_I\kappa_1^2 + {}_I K_8\,{}_I\kappa_2^1\}\mathbf{e}_1 + {}_I L\{{}_I K_4\,{}_I\kappa_1^1 + {}_I K_5\,{}_I\kappa_2^2\}\mathbf{e}_2 + W\{K_2\,{}_I\kappa_2^3\}\mathbf{e}_3],\\
{}_I\check{\mathbf{t}}^4 &= {}_I V[\tfrac{1}{2}{}_I\eta_3(\mathbf{e}_2\cdot{}_I\dot{\boldsymbol{\delta}}_4)\mathbf{e}_2 + {}_I\eta_4(\mathbf{e}_3\cdot{}_I\dot{\boldsymbol{\delta}}_4)\mathbf{e}_3],\\
{}_I\check{\mathbf{t}}^5 &= {}_I V[\tfrac{1}{2}{}_I\eta_3(\mathbf{e}_1\cdot{}_I\dot{\boldsymbol{\delta}}_5)\mathbf{e}_1 + {}_I\eta_5(\mathbf{e}_3\cdot{}_I\dot{\boldsymbol{\delta}}_5)\mathbf{e}_3],\\
{}_I\hat{\mathbf{t}}^i &= [{}_I d^{1/2}\,{}_I\hat{\mathbf{T}}]\cdot\mathbf{e}_i, \quad {}_I\check{\mathbf{t}}^i = [{}_I d^{1/2}\,{}_I\check{\mathbf{t}}]\cdot\mathbf{e}_i \quad \text{for } i = 1,2,3.
\end{aligned}
\tag{60}
$$

Moreover, the assigned fields Eq. (28) are given by

$$
{}_I m_I\mathbf{B}^0 = {}_I m\alpha g\mathbf{e}_3, \quad {}_I m_I\mathbf{B}_i = 0 \quad \text{for } i = 1,2,\ldots,5,
\tag{61}
$$

where it is noted that the aerodynamic term is quadratic in velocity so that it vanishes in the linearized theory. Thus, the equations of motion (30) yield

$$
\begin{aligned}
{}_I\mathbf{m}_1^0 &= \frac{1}{{}_I L}\left[\frac{{}_I L}{2}\{{}_I m_I\ddot{\boldsymbol{\delta}}_0 - {}_I m_I\mathbf{B}^0\} - \{{}_I m_I y^{33}\,{}_I\ddot{\boldsymbol{\delta}}_3 + {}_I\mathbf{t}^3\}\right],\\
{}_I\mathbf{m}_2^0 &= \frac{1}{{}_I L}\left[\frac{{}_I L}{2}\{{}_I m_I\ddot{\boldsymbol{\delta}}_0 - {}_I m_I\mathbf{B}^0\} + \{{}_I m_I y^{33}\,{}_I\ddot{\boldsymbol{\delta}}_3 + {}_I\mathbf{t}^3\}\right],\\
{}_I\mathbf{m}_1^1 &= \frac{1}{{}_I L}\left[\frac{{}_I L}{2}\{{}_I m_I y^{11}\,{}_I\ddot{\boldsymbol{\delta}}_1 + {}_I\mathbf{t}^1\} - \{{}_I m_I y^{44}\,{}_I\ddot{\boldsymbol{\delta}}_4 + {}_I\mathbf{t}^4\}\right],\\
{}_I\mathbf{m}_2^1 &= \frac{1}{{}_I L}\left[\frac{{}_I L}{2}\{{}_I m_I y^{11}\,{}_I\ddot{\boldsymbol{\delta}}_1 + {}_I\mathbf{t}^1\} + \{{}_I m_I y^{44}\,{}_I\ddot{\boldsymbol{\delta}}_4 + {}_I\mathbf{t}^4\}\right],\\
{}_I\mathbf{m}_1^2 &= \frac{1}{{}_I L}\left[\frac{{}_I L}{2}\{{}_I m_I y^{22}\,{}_I\ddot{\boldsymbol{\delta}}_2 + {}_I\mathbf{t}^2\} - \{{}_I m_I y^{55}\,{}_I\ddot{\boldsymbol{\delta}}_5 + {}_I\mathbf{t}^5\}\right],\\
{}_I\mathbf{m}_2^2 &= \frac{1}{{}_I L}\left[\frac{{}_I L}{2}\{{}_I m_I y^{22}\,{}_I\ddot{\boldsymbol{\delta}}_2 + {}_I\mathbf{t}^2\} + \{{}_I m_I y^{55}\,{}_I\ddot{\boldsymbol{\delta}}_5 + {}_I\mathbf{t}^5\}\right].
\end{aligned}
\tag{62}
$$

Also, the linearized form of the kinematic boundary conditions (43) become

$$
{}_1\boldsymbol{\delta}_0^* = R\phi\mathbf{e}_1, \quad {}_1\boldsymbol{\delta}_1^* = -\phi\mathbf{e}_3, \quad {}_1\boldsymbol{\delta}_2^* = 0
\tag{63}
$$

and initial conditions need to be specified for the quantities

$$
\{{}_I\boldsymbol{\delta}_i^*(0), \quad {}_I\dot{\boldsymbol{\delta}}_i^*(0)\} \quad \text{for } (I = 1,2,\ldots,N+1; \ \ i = 0,1,2).
\tag{64}
$$

In addition, linearization of Eq. (37) yields

$$
\begin{aligned}
{}_{I+1}\check{\mathbf{m}} &= \mathbf{e}_1\times\left[\frac{1}{2}{}_I\check{\mathbf{t}}^1 + \frac{I}{{}_I L}{}_I\check{\mathbf{t}}^4\right] + \mathbf{e}_2\times\left[\frac{1}{2}{}_I\check{\mathbf{t}}^2 + \frac{I}{{}_I L}{}_I\check{\mathbf{t}}^5\right]\\
&= \frac{1}{2}[\mathbf{e}_1\times{}_I\check{\mathbf{t}}^1 + \mathbf{e}_2\times{}_I\check{\mathbf{t}}^2] + \frac{{}_I V}{{}_I L}\Big[{}_I\eta_5(\mathbf{e}_3\cdot{}_I\dot{\boldsymbol{\delta}}_5)\mathbf{e}_1\\
&\quad -{}_I\eta_4(\mathbf{e}_3\cdot{}_I\dot{\boldsymbol{\delta}}_4)\mathbf{e}_2 + \frac{1}{2}{}_I\eta_3\{(\mathbf{e}_2\cdot{}_I\dot{\boldsymbol{\delta}}_4) - (\mathbf{e}_1\cdot{}_I\dot{\boldsymbol{\delta}}_5)\}\mathbf{e}_3\Big],
\end{aligned}
\tag{65}
$$

which shows that the viscosities of torsion and two bending modes can be determined independently.

Now, with the help of Eqs. (58)–(60) and (62), the kinetic coupling equation (31), the kinematic boundary conditions (63) and the kinetic boundary conditions (44) yield $3(N+1)$ vectors equations to determine the $3(N+1)$ nodal director displacements ${}_I\boldsymbol{\delta}_i^*$. The resulting system of equations represents a set of linear ordinary differential equations, which are second order in time with constant coefficients. The system can be solved using standard methods, which introduce auxiliary variables to develop an equivalent set of $6(N+1)$

Table 1
Values of the viscosity coefficients of damping, beam and mass elements and the drag coefficient of the mass

	Damping element $I=1$	Beam elements $I=2,3,\ldots,M+1$	Mass element $I=N$
${}_I\eta_1$ (MPa s)	3	3	30
${}_I\eta_2$ (MPa s)	2	2	20
${}_I\eta_3$ (MN s)	0.1	0.1	100
${}_I\eta_4$ (MN s)	50	1	100
${}_I\eta_5$ (MN s)	300	0.05	100
C_D	—	—	4
ρ_a (g/m^3)	—	—	1.05

first-order vector differential equations. Since material dissipation has been included, the real parts of the solutions of the resulting modal equations are composed of a particular part that oscillates with the forcing frequency ω, and a transient homogeneous part that exhibits sinusoidal oscillation with exponential decay. In particular, the transient part of the nth modal solution takes the standard form

$$A_n \exp(-\zeta_n\omega_n t)\sin(\omega_n t+\Phi_n), \tag{66}$$

where A_n is its magnitude, ω_n is its natural frequency, ζ_n is its normalized damping coefficient and Φ_n is its phase angle.

In Ref. [1], measurements of the natural frequencies and damping coefficients were made of the first modes of bending in the weak and strong bending planes and of torsion, as well as of the second mode of bending in the weak bending plane. The coefficients $\{{}_I\eta_1,\ {}_I\eta_2\}$ control damping of homogeneous deformations, which were not measured in the experiments. Consequently, the values given in Table 1 were specified by taking

$${}_I\eta_1=\frac{2}{3}{}_I\eta_2 \tag{67}$$

and by specifying ${}_I\eta_2$ to be reasonably small.

As previously mentioned, aerodynamic drag is a nonlinear phenomena that does not affect the linear solution. The values of the density ρ_a of air and the drag coefficient C_D given in Table 1 for the nonlinear response were determined by tables in Ref. [18], with the value of C_D being restricted to be consistent with the known range of values associated with the velocity of the mass that was on the order of 0.5 m/s.

For all cases, the elastic properties $\{E^*,v^*\}$ of each element are the same. The damping coefficients in the first element ($I=1$) are used to model damping in the experimental setup, the damping coefficients in each of the beam elements ($I=2,3,\ldots,N-1$) are the same, and the damping coefficients in the mass element ($I=N$) are taken to be large in order to simulate the mass as a nearly rigid body. More specifically, by specifying values for the coefficients $\{{}_I\eta_3,\ {}_I\eta_4,\ {}_I\eta_5\}$ and solving the linearized equations it is possible to predict the natural frequencies of vibration and the normalized damping coefficient ζ of each mode of vibration.

The values of the coefficients $\{{}_I\eta_3,\ {}_I\eta_4,\ {}_I\eta_5\}$ were calibrated by matching the measured damping coefficients for the first torsion mode and the first bending modes in the strong and weak directions of the beam–mass system reported in Ref. [1]. The calibration procedure for determining the damping coefficients $\{{}_1\eta_3,\ {}_1\eta_4,\ {}_1\eta_5\}$ in the first element and the damping coefficients $\{{}_2\eta_3,\ {}_2\eta_4,\ {}_2\eta_5\}$ in the beam elements used the following two steps. For step 1, the short first element was eliminated and the values of $\{{}_2\eta_3,\ {}_2\eta_4\}$ associated with the beam elements were determined to match the experimentally determined damping values for the first torsion mode and the first bending mode in the strong bending direction. The value $\{{}_2\eta_5\}$ controlling the damping of the first bending mode in the weak bending direction was specified to be a reasonably low value associated with steel and was not calibrated to yield the high value measured in the experimental setup. For the final step 2, the full numerical model with the short first element was used and the damping coefficients $\{{}_2\eta_3,\ {}_2\eta_4,\ {}_2\eta_5\}$ of the beam elements ($I=2,3,\ldots,N-1$) were set equal to the values determined in step 1. Then, the values of $\{{}_1\eta_3,\ {}_1\eta_4,\ {}_1\eta_5\}$ were determined to match the experimentally determined damping values for the first torsion

Table 2
Measured and predicted natural frequencies and damping coefficients for the first four modes of vibration ($\alpha = 1$)

Mode type	Exp. (Hz)	Linear theory (Hz)	Nonlinear theory (Hz)	Exp. ζ (%)	Linear theory ζ (%)
First bending mode (weak plane)	2.76	2.36	2.70	4.0	5.67
First bending mode (strong plane)	26.75	28.27	29.55	0.187	0.17
Torsional mode	41.82	41.15	40.4	0.119	0.24
Second bending mode (weak plane)	44.03	44.91	—	0.05	0.6

Table 3
Effect of gravity

α	Measured frequency (Hz)	Simple model frequency (Hz)	Nonlinear theory frequency (Hz)
1	2.76	2.73	2.70
0	2.35	2.45	2.36
−1	1.87	2.07	1.82

Measured natural frequencies of the first bending mode in the weak bending plane and theoretical predictions of the simple model in Ref. [1] and simulations of the nonlinear theory for different values of α.

mode and both the first bending modes in the strong and weak bending directions. Consequently, the value $\{{}_1\eta_5\}$ models the high damping measured in the experimental setup for the first bending mode in the weak bending direction, which was influenced by damping in the extension bar and bearings. The calibrated values of the coefficients summarized in Table 1 are used in the remaining simulations discussed in this paper.

Table 2 lists the natural frequencies and the normalized damping coefficients ζ measured in the experiments and determined by the linearized equations with the viscosity coefficients in Table 1. Table 2 also includes the natural frequencies predicted by simulations of the nonlinear equations with appropriate initial conditions, which cause small deformations in the desired modes. In particular, it is noted that with the help of the damping element ($N = 1$) the damping coefficients of the resulting theory are in reasonable agreement with those of the experiment. Also, it can be seen that the linearized theory cannot capture the stiffening effect of gravity for the first bending mode in the weak bending plane that is observed in the experimental data and in the small deformation simulation of the nonlinear equations. Table 3 compares the experimental data with the results of the simple model in Ref. [1] and the results of small deformation simulations of the nonlinear equations. From this table, it can be seen that the nonlinear equations accurately predict the natural frequencies for the case when the mass is oriented below the beam's clamped end ($\alpha = 1$, as in Table 2); for the case of no gravity ($\alpha = 0$); and for the case when the mass is oriented above the beam's clamped end ($\alpha = -1$).

6. A preliminary example problem

The accuracy of the numerical simulations of the nonlinear equations of the theory of a Cosserat point was studied to determine limitations on the maximum time step Δt for the Newmark integration scheme discussed in Section 4 and for the minimum number M of elements in the spatial discretization of the beam. In this regard, it is recalled that the beam–mass system was discretized into $N = M + 2$, with one damping element ($I = 1$), M equal beam elements and one ($I = N$) element for the mass (at the end of the beam) whose behavior was dominated by near rigid body motion.

In order to determine the maximum time step, a simple problem was considered in which the beam–mass system was initially in its stress-free reference configuration, the centroids of the cross-sections were subjected to linear velocity gradients in two directions and the clamped end remained fixed. For this case, the nodal

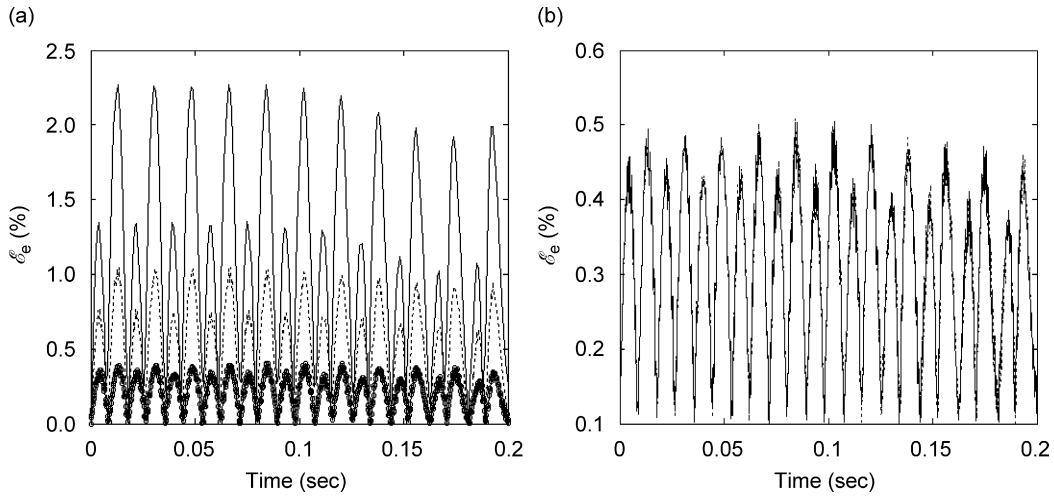

Fig. 3. Plots of the error $\mathscr{E}_e$ Eq. (70) in the total energy as functions of time: for different values of the time step Δt with $M = 16$ (the number of beam elements); and (b) for different values of M with $\Delta t = 20\,\mu s$. The curve labels are: (a) —— $\Delta t = 100\,\mu s$; · · · · · $\Delta t = 50\,\mu s$; —o— $\Delta t = 20\,\mu s$; (b) —— $M = 16$; · · · · · $M = 32$.

Table 4
Excitation frequencies and amplitudes specified in the experiments and in the simulations

Response	ω (Hz) exp. and sim.	ϕ_0 (deg) exp.	ϕ_0 (deg) sim.
Torsion I	35.0	1.11	0.9
Torsion II	27.0	1.50	1.0
Bending II	35.0	1.11	0.9

director vectors and their velocities were specified by

$$
\begin{aligned}
&{}_I\mathbf{d}_i^*(0) = {}_I\mathbf{D}_i^* \quad \text{for } i = 0,1,2, \quad {}_I\mathbf{w}_0^*(0) = \left[\frac{(|{}_I\mathbf{D}_0^*| - R)}{(|{}_{N+1}\mathbf{D}_0^*| - R)}\right][V_1\mathbf{e}_1 + V_2\mathbf{e}_2],\\
&{}_I\mathbf{w}_1^*(0) = {}_I\mathbf{w}_2^*(0) = 0 \quad \text{for } I = 1,2,\ldots,N+1,
\end{aligned}
\tag{68}
$$

where $V_1 = 0.387\,\text{m/s}$ and $V_2 = 6.45\text{E}{-4}\,\text{m/s}$. These values of V_1 and V_2 cause large deformations of the system, which are on the order of those being studied in the experiments. Moreover, in the absence of gravity and damping ($\alpha = 0$; ${}_I\eta_i = 0$, ${}_IC_D = 0$) the beam–mass system is free of external loads except at the clamped end, which is fixed so that the total energy $\mathscr{E}$

$$
\mathscr{E} = \mathscr{K} + \mathscr{U} \tag{69}
$$

remains constant with time. Consequently, the accuracy of the numerical integration scheme can be examined by considering the error $\mathscr{E}_e$ in the total energy defined by

$$
\mathscr{E}_e = \frac{\mathscr{E} - \mathscr{E}_0}{\mathscr{E}_0}. \tag{70}
$$

Fig. 3a plots this error as a function of time for different values of the time step Δt with $M = 16$ equal beam elements and Fig. 3b plots the same error estimate for $\Delta t = 20\,\mu s$ and two values of the discretization M of the beam. These results indicate that the numerical scheme is reasonably converged for this example.

For the simulations described here and in the next section it is recalled from Ref. [1] that the controller in the experiments could not maintain a constant amplitude nor a pure sine function as the excitation equation (1) of the beam when dynamic buckling occurred. Therefore, in comparing the simulations with the experiments, the

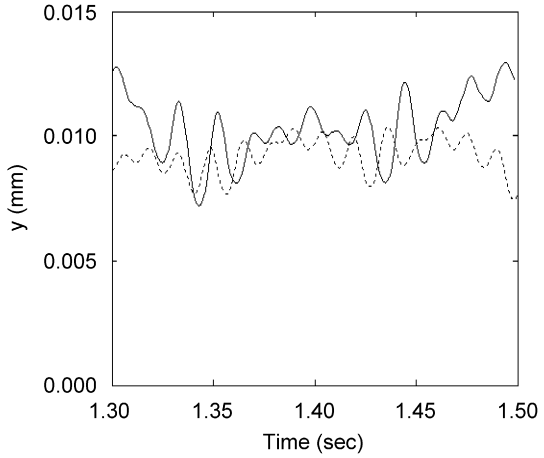

Fig. 4. Torsion I: Plots of the out-of-plane component $(\mathbf{e}_2 \cdot {}_N\mathbf{d}_0^*)$ of the centroid of the beam's end as a function of time for different values of the number M of beam elements with $\Delta t = 20\,\mu s$. The curve labels are: · · · · · $M = 16$; —— $M = 32$.

excitation frequency ω was taken to be the same as that in the experiments but the excitation amplitude ϕ_0 was adjusted to better match the amplitudes of motion of the mass measured in the experiments. Table 4 summarizes the excitation frequencies and amplitudes specified in the experiments in Ref. [1] and those used in the simulations reported here.

In order to determine the minimum number M of beam elements for accurate spatial resolution, simulations were considered for the response Torsion I with an excitation amplitude $\phi_0 = 0.65^\circ$ and frequency $\omega = 35.0\,Hz$, including gravity, the damping element ($I = 1$), material damping in the beam elements and aerodynamic drag on the mass element. Fig. 4 plots the out-of-plane component $(\mathbf{e}_2 \cdot {}_N\mathbf{d}_0^*)$ of the centroid of the beam's end which is attached to the mass as a function of time for two different values of M with $\Delta t = 20\,\mu s$. The results shown in Fig. 4 indicate that the differences between the solutions for the meshes $M = 16$ and 32 are much more significant than those observed in Fig. 3b for the same time step $\Delta t = 20\,\mu s$. In this regard, it is emphasized that the simulation in Fig. 3 has no energy input and no dissipation, whereas the simulation of Torsion I in Fig. 4 includes both energy input and dissipation. Therefore, the results in Fig. 4 represent a complicated balance of nonlinear phenomena. In particular, it is observed that the results in Fig. 4 are consistent with those in the experiment, which indicate that the center of the mass remains on one side of the vertical $(\mathbf{e}_1$–$\mathbf{e}_3)$ plane. Also, it can be seen from Fig. 4 that the average amplitude of the lateral displacement is relatively unchanged by increasing the number of elements in the simulation. The decision to use $M = 16$ with $\Delta t = 20\,\mu s$ for the remainder of the simulations in this paper was partially based on the necessity to reduce the computation effort required to simulate the long-time response of the experiments using a small time step. This decision was also based on the fact that the model with $M = 16$ elements is capable of capturing the main nonlinear responses observed in the experiments for Torsions I and II and Bending II, which were found to be quite difficult to simulate with a specified set of material and damping parameters.

7. Comparions of simulations with experimental data

It will be shown presently that the theory of a Cosserat point can be used to simulate most of the experimental data with reasonable accuracy. Also, with the help of the damping element the simulations are able to capture the extensive damping of the first mode of bending in the weak bending plane observed in the experiments of Torsions I and II. However, the simulations do not accurately predict the results of Torsion III. A small initial perturbation was used for all of the simulations. Specifically, for the responses Torsion I–III the initial conditions were specified so that the beam and mass were pre-twisted with

zero initial velocity

$$
\begin{aligned}
&{}_1\mathbf{d}_0^*(0) = {}_1\mathbf{D}_i^* \quad \text{for } i = 0,1,2, \quad {}_1\mathbf{w}_0^*(0) = R\phi_0\omega\mathbf{e}_1, \quad {}_1\mathbf{w}_1^*(0) = -\phi_0\omega\mathbf{e}_3, \quad {}_1\mathbf{w}_2^*(0) = 0,\\
&{}_I\mathbf{d}_0^*(0) = {}_I\mathbf{D}_0^*, \quad {}_I\mathbf{d}_1^*(0) = \left[\frac{(|{}_I\mathbf{D}_0^*| - R)}{(|{}_{N+1}\mathbf{D}_0^*| - R)}\right][\cos\Theta\mathbf{e}_1 + \sin\Theta\mathbf{e}_2],\\
&{}_I\mathbf{d}_2^*(0) = \left[\frac{(|{}_I\mathbf{D}_0^*| - R)}{(|{}_{N+1}\mathbf{D}_0^*| - R)}\right][-\sin\Theta\mathbf{e}_1 + \cos\Theta\mathbf{e}_2],\\
&{}_I\mathbf{w}_i^*(0) = 0 \quad \text{for } I = 1,2,\ldots,N+1 \text{ and } i = 0,1,2,
\end{aligned}
\tag{71}
$$

where the torsion angle $\Theta = 1^\circ$ and the initial velocity field is consistent with the boundary condition (43). Also, for the simulation of Bending II, initial conditions of the forms Eq. (68) were used with $V_1 = 0\,\text{m/s}$ and $V_2 = 6.45\text{E}{-4}\,\text{m/s}$, which by themselves cause small deflections.

The camera angle used in the experiments reported in Ref. [1] prevented the accurate measurement of displacements in the $\mathbf{e}_1$ direction. Therefore, the analysis of the torsion angle used an approximation, which assumed that this displacement was reasonably small. In order to compare with this experimental data, this same approximation is used to analyze the results of the simulations. Specifically, let ${}_N\theta$ be the approximate value of the torsion angle at the beam's end, which is attached to the mass. To develop an expression for ${}_N\theta$ it is convenient to define an auxiliary orthonormal triad $\mathbf{e}_i'$ associated with the beam's end, such that

$$
\mathbf{e}_1' = \mathbf{e}_1, \;\; \mathbf{e}_2' = \mathbf{e}_3' \times \mathbf{e}_1', \;\; \mathbf{e}_3' = \frac{{}_N\mathbf{d}_3^* - ({}_N\mathbf{d}_3^* \cdot \mathbf{e}_1)\mathbf{e}_1}{|{}_N\mathbf{d}_3^* - ({}_N\mathbf{d}_3^* \cdot \mathbf{e}_1)\mathbf{e}_1|}, \quad {}_N\mathbf{d}_3^* = {}_N\mathbf{d}_1^* \times {}_N\mathbf{d}_2^*, \tag{72}
$$

where ${}_N\mathbf{d}_3^*$ is normal to the cross-section of the beam's end, and $\mathbf{e}_3'$ is the unit vector in the direction of the projection of this normal into the vertical plane normal to $\mathbf{e}_1$. Next, the projections $\{{}_N\bar{\mathbf{d}}_1^*, {}_N\bar{\mathbf{d}}_2^*\}$ of the nodal vectors into the $\mathbf{e}_1' - \mathbf{e}_2'$ plane are specified by

$$
{}_N\bar{\mathbf{d}}_1^* = {}_N\mathbf{d}_1^* - ({}_N\mathbf{d}_1^* \cdot \mathbf{e}_3')\mathbf{e}_3', \quad {}_N\bar{\mathbf{d}}_2^* = {}_N\mathbf{d}_2^* - ({}_N\mathbf{d}_2^* \cdot \mathbf{e}_3')\mathbf{e}_3', \tag{73}
$$

so that the torsion angle ${}_N\theta$ at the beam's end can be approximated by the expressions

$$
\begin{aligned}
&{}_N\theta = \tfrac{1}{2}({}_N\theta_1 + {}_N\theta_2),\\
&{}_N\theta_1 = \tan^{-1}\left[\frac{{}_N\bar{\mathbf{d}}_1^* \cdot \mathbf{e}_2'}{{}_N\bar{\mathbf{d}}_1^* \cdot \mathbf{e}_1'}\right], \quad {}_N\theta_2 = -\tan^{-1}\left[\frac{{}_N\bar{\mathbf{d}}_2^* \cdot \mathbf{e}_1'}{{}_N\bar{\mathbf{d}}_2^* \cdot \mathbf{e}_2'}\right].
\end{aligned}
\tag{74}
$$

In the following comparisons with the experimental data use is made of the constants reported in the tables in Ref. [1], which provide analytical expressions for parametric functions of time and polynomial functions of space that yield smooth fits of the raw experimental data.

Figs. 5–7 compare predictions of the numerical simulations with results of the experimental data, respectively, for Torsions I and II, and Bending II in Ref. [1]. Figs. 5a, 6a, 7a show the values of $(\mathbf{e}_2 \cdot {}_N\mathbf{d}_0^*)$ associated with the out-of-plane motion of the centroid of the beam's end; Figs. 5b, 6b, 7b compare the predictions of the torsion angle ${}_N\theta$ of the beam's end with the parametric approximations of the experimental data; and Figs. 5c, 6c, 7c compare the shapes of the centroid of the beam in the simulations with the polynomial approximations of the experiments for different times. In general, the results in Figs. 5–7 show reasonably good agreement with the experimental data.

In the experiments Torsions I–III described in Ref. [1] it was observed that the damping in the weak bending plane was high enough to keep the end of the beam (attached to the mass) nearly stationary on one side of the vertical plane as the beam oscillated. The results in Figs. 5a and 6a show that the simulations predict that the beam's end remains on one side of the vertical plane but they exhibit an additional oscillation of magnitude 1 mm (Fig. 5a) and 4 mm (Fig. 6a) at a frequency of about 3.5 Hz, which is near the frequency of first mode of bending in the weak bending plane. The simulation of Torsion III, which is not shown here, cannot capture this phenomena since in the simulation the beam's end oscillates on both sides of the vertical plane. The fact that the experiments do not exhibit this low-frequency oscillations may be partially due to added damping in the experimental system and the inability of the controller to maintain a sinusoidal excitation during dynamic buckling.

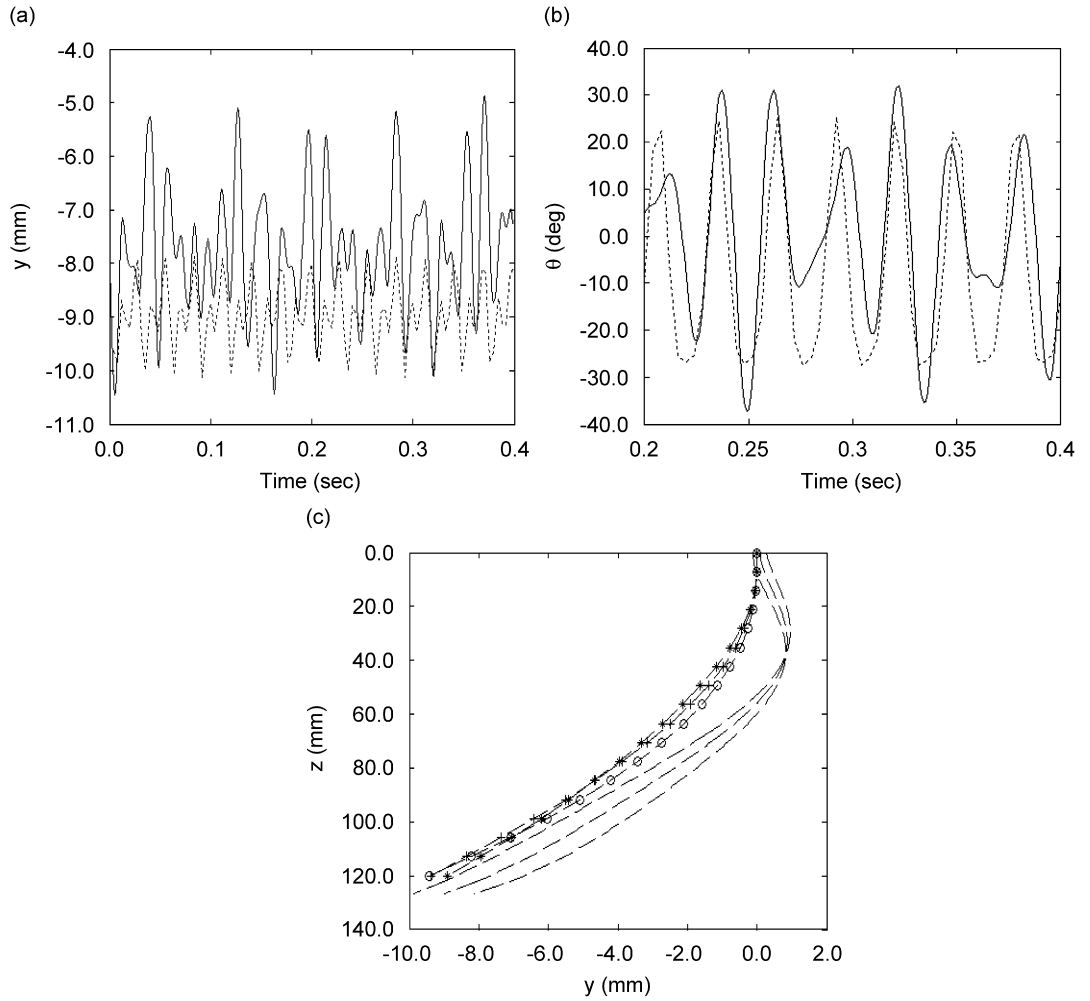

Fig. 5. Torsion I: Comparison of the simulations and the experimental data. The curve labels are: (a, b) · · · · · Exp.; ——Sim.; (c) —o— Sim. 0 ms; —+— Sim. 8 ms; —*— Sim. 16 ms; · · · · · Exp.

8. Comparison with ansys

It is of interest to compare the predictions of the Cosserat model with those of the nonlinear beam element BEAM 189 in the commercial program ANSYS [19]. In the previous section it was found that the results of the simulations of the responses to the torsional modes are sensitive to the magnitude of damping. Therefore, in order to perform a representative simulation in ANSYS it is necessary to determine damping coefficients. These coefficients in ANSYS have forms based on linearized equations of motion which can be written as

$$\mathbf{M}\ddot{\mathbf{x}} + \mathbf{C}\dot{\mathbf{x}} + \mathbf{K}\mathbf{x} = 0, \tag{75}$$

where $\mathbf{x}$ is the vector of unknowns, $\mathbf{M}$ the symmetric mass matrix, $\mathbf{K}$ the symmetric stiffness matrix and $\mathbf{C}$ the damping matrix. Specifically, ANSYS admits a damping matrix $\mathbf{C}$ of the form

$$\mathbf{C} = \eta_M \mathbf{M} + \eta_K \mathbf{K}, \tag{76}$$

where $\{\eta_M, \eta_K\}$ are damping coefficients. The linearized equations of the theory of a Cosserat point developed in Section 5 yield a different damping matrix $\mathbf{C}$ from that obtained by the form equation (76). In this regard, it is noted that the constitutive Eq. (26) have been motivated by the desire to model damping of physical structural modes of vibration of the element instead of by the pure mathematical convenience of being able

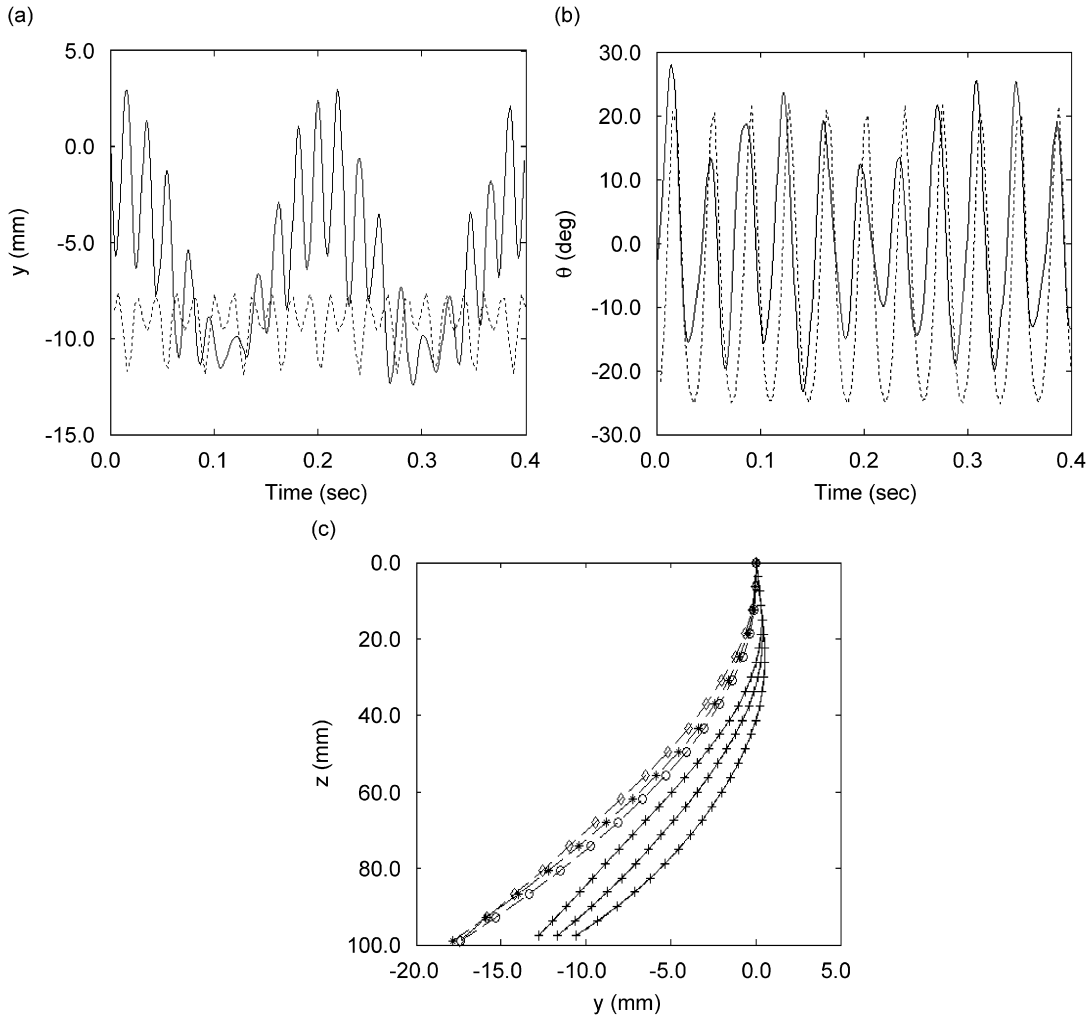

Fig. 6. Torsion II: Comparison of the simulations and the experimental data. The curve labels are: (a, b) · · · · · Exp.; —Sim.; (c) —o— Sim. 0 ms; —+— Sim. 12 ms; —*— Sim. 24 ms; · · · · · Exp.

to diagonalize the resulting damped system of equations. Consequently, in order to calibrate the constants $\{\eta_M, \eta_K\}$ for the ANSYS model, the damping matrix $\mathbf{C}$ obtained from the Cosserat theory of Section 5 was replaced by the form equation (76), the short damping element was eliminated and the resulting equations were solved to obtain values for the natural frequencies and the normalized damping coefficients of the first four modes of vibration. The calibrated values of $\{\eta_M, \eta_K\}$ are given in Table 5a and the associated predictions of the resulting linearized equations (in the absence of gravity, $\alpha = 0$) are given in Table 5b, where comparison is also made with the results using the linearized equations of the full Cosserat model (including the short damping element) together with the viscosity coefficients given in Table 1. Since the values of the constants $\{\eta_M, \eta_K\}$ affect all modes it is only possible to match the Cosserat results in an average sense.

An ANSYS simulation of Torsion I was performed using a discretization with no short damping element, 16 equal beam elements and 1 mass element and using the damping coefficients in Table 5a. Also, the effect of gravity ($\alpha = 1$) was included and the boundary condition at the clamped end was the same Eq. (43) as that used on the clamped end of the damping element in the Cosserat simulations. Fig. 8 compares the simulations of the full Cosserat model (with the short damping element) and the ANSYS model for the motion of the centroid ($\mathbf{e}_2 \cdot {}_N\mathbf{d}_0^*$) (Fig. 8a) and the torsion angle ${}_N\theta$ (Fig. 8b) at the beam's end for Torsion I. Although the ANSYS model had more damping in the first bending mode in the weak bending plane than the Cosserat

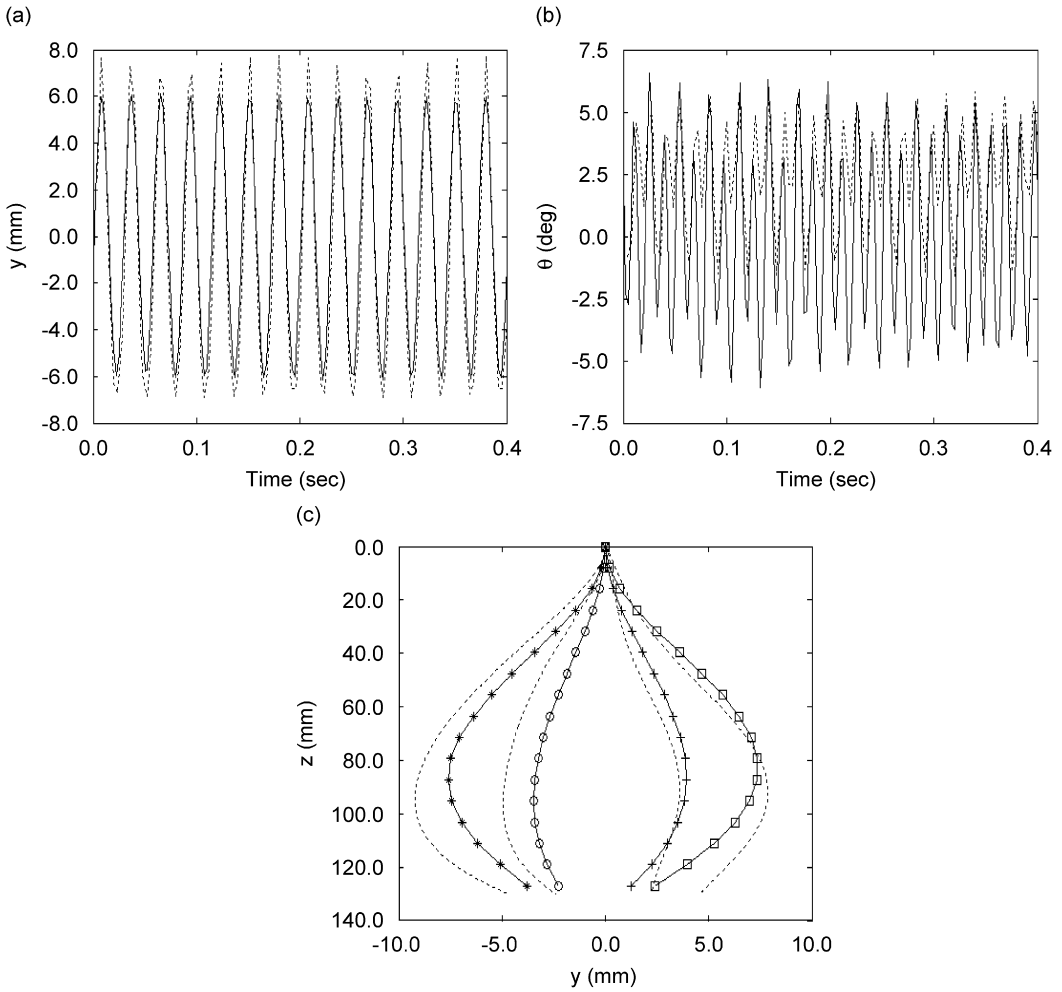

Fig. 7. Bending II: Comparison of the simulations and the experimental data. The curve labels are: (a, b) · · · · · Exp.; —— Sim.; (c) —o— Sim. 0 ms; —+— Sim. 7 ms; —*— Sim. 14 ms; —◇— Sim. 21 ms; · · · · · Exp.

Table 5a
Values of the damping coefficients used in ANSYS

η_M (s^{-1})	2
η_K (s)	0.0001

Table 5b
Natural frequencies and damping coefficients for the first four modes of vibration based on the linearized equations using the coefficients for the Cosserat and ANSYS models (with $\alpha = 0$)

Mode type	Cosserat (Hz)	ANSYS (Hz)	Cosserat ζ (%)	ANSYS ζ (%)
First bending mode (weak plane)	2.357	2.383	5.67	5.81
First bending mode (strong plane)	28.27	28.58	0.17	1.37
Torsional mode	41.15	42.30	0.24	1.62
Second bending mode (weak plane)	44.91	45.30	0.6	1.71

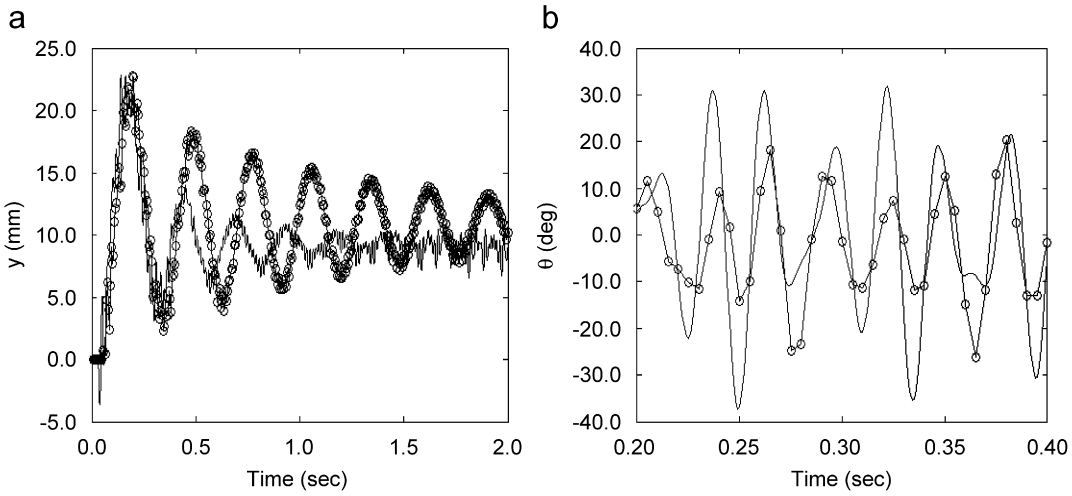

Fig. 8. Torsion I: Comparison of the simulations of the Cosserat and ANSYS models for (a) the centroid ($\mathbf{e}_2 \cdot {}_N\mathbf{d}_0^*$) and (b) the torsion angle ${}_N\theta$ at the beam's end. The curve labels are: — Cosserat; —o— ANSYS.

model, the ANSYS calculation took longer to reach near steady state. In particular, it is noted that the ANSYS simulation also exhibits oscillations of the centroid of the beam's end at a low frequency near that of the first bending mode in the weak bending plane.

9. Conclusions

The theory of a Cosserat point has been used to develop a numerical model for the nonlinear dynamic response of an elastic beam–mass system with viscous damping and aerodynamic drag. The Cosserat equations have been solved using the Newmark time-integration scheme and an analytical expression for the tangent stiffness of the resulting Newton–Raphson iteration procedure has been developed. Comparison with the experimental data in Ref. [1] shows that the Cosserat model accurately predicts the nonlinear stiffening and weakening effect of gravity when the mass is located below and above the beam's clamped end, respectively.

The simulations reproduce the experimental result that two different nonlinear modes of vibration (Torsion I and Bending II) occur at the same excitation amplitude and frequency. Torsion I is a dynamic lateral torsional post-buckling mode associated with out-of-plane motion of the beam–mass system which is dominated by oscillating torsion of the beam. Bending II is dominated by a nonlinear second bending mode in the weak bending plane. The simulations of the Cosserat model are in reasonably good quantitative agreement with the experimental results for these two modes of vibration.

For the responses Torsions I–III the end of beam remained on one side of the vertical plane. The simulations were able to capture this phenomena for Torsion I and II but not for Torsion III. Moreover, the simulations indicated a low-frequency oscillation in the weak bending plane, which was not observed in the experiments. Damping of this mode in the experiments is presumed to be due to flexibility of the extension bar, damping in the bearings and effects of the controller, and is modeled by a small damping element located at the clamped end of the beam. Also, simulations were performed for Torsions I and II in which the effect of aerodynamic drag on the mass was eliminated. The results indicated that aerodynamic drag has a significant effect and cannot be neglected.

Even though the Cosserat theory was not able to accurately simulate the results of Torsion III, which produced the largest amplitude vibrations, the Cosserat simulations were in reasonably good agreement with the experimental data for Torsions I and II. This demonstrates that the simulations capture the experimental observation that similar post-buckling responses can occur for a range of excitation amplitudes and frequencies.

Comparison was also made with the commercial code ANSYS for simulations of Torsion I, which indicate similar results to those of the Cosserat simulation with a persistent oscillation of the centroid of the beam's end at a low frequency near that of the first bending mode in the weak bending plane.

Acknowledgments

The research of M.B. Rubin was partially supported by his Gerard Swope Chair in Mechanics and the fund for the promotion of research at the Technion. Also, the authors would like to acknowledge helpful discussions with H. Flasher.

Appendix A. Details of the tangent stiffness

The objective of this Appendix A is to present explicit expressions for the tensors $\{{}_I\hat{\mathbf{K}}^{ij}, {}_I\check{\mathbf{K}}^{ij}, {}_I\mathbf{N}^{0j}, {}_I\mathbf{M}_\alpha^{ij}\}$, which determine the tensors in Eq. (57) associated with the tangent stiffness Eq. (51). To this end, it is convenient to generalize the definition of the Kronecker delta, such that

$$\delta_m^j = 1 \quad \text{for } m = j, \quad \delta_m^j = 0 \quad \text{for } m \neq j \quad \text{with } m, j = 0, 1, \ldots, 5. \tag{77}$$

Then, with the help of Eqs. (13), (28), (30), (41) and (54) it follows that

$$\begin{aligned}
{}_I\mathbf{M}_1^{0j} &= \frac{1}{2}[{}_I m a_3 \delta_0^j \mathbf{I} - {}_I\mathbf{N}^{0j}] - \frac{1}{{}_I L}[{}_I m_I y^{33} a_3 \delta_3^j \mathbf{I} + {}_I\mathbf{K}^{3j}],\\
{}_I\mathbf{M}_2^{0j} &= \frac{1}{2}[{}_I m a_3 \delta_0^j \mathbf{I} - {}_I\mathbf{N}^{0j}] + \frac{1}{{}_I L}[{}_I m_I y^{33} a_3 \delta_3^j \mathbf{I} + {}_I\mathbf{K}^{3j}],\\
{}_I\mathbf{M}_1^{1j} &= \frac{1}{2}[{}_I m_I y^{11} a_3 \delta_1^j \mathbf{I} + {}_I\mathbf{K}^{1j}] - \frac{1}{{}_I L}[{}_I m_I y^{44} a_3 \delta_4^j \mathbf{I} + {}_I\mathbf{K}^{4j}],\\
{}_I\mathbf{M}_2^{1j} &= \frac{1}{2}[{}_I m_I y^{11} a_3 \delta_1^j \mathbf{I} + {}_I\mathbf{K}^{1j}] + \frac{1}{{}_I L}[{}_I m_I y^{44} a_3 \delta_4^j \mathbf{I} + {}_I\mathbf{K}^{4j}],\\
{}_I\mathbf{M}_1^{2j} &= \frac{1}{2}[{}_I m_I y^{22} a_3 \delta_2^j \mathbf{I} + {}_I\mathbf{K}^{2j}] - \frac{1}{{}_I L}[{}_I m_I y^{55} a_3 \delta_5^j \mathbf{I} + {}_I\mathbf{K}^{5j}],\\
{}_I\mathbf{M}_1^{2j} &= \frac{1}{2}[{}_I m_I y^{22} a_3 \delta_2^j \mathbf{I} + {}_I\mathbf{K}^{2j}] + \frac{1}{{}_I L}[{}_I m_I y^{55} a_3 \delta_5^j \mathbf{I} + {}_I\mathbf{K}^{5j}],\\
&\text{for } j = 0, 1, \ldots, 5 \quad \text{and} \quad I = 1, 2, \ldots, N,
\end{aligned} \tag{78}$$

where it is noted that the constant body force does not influence the tangent stiffness, and use has been made of Eq. (47) to deduce that

$$\Delta({}_I\mathbf{w}_m) = \sum_{j=0}^{5} a_1 a_3 \delta_m^j \Delta({}_I\mathbf{d}_j), \quad \Delta({}_I\dot{\mathbf{w}}_m) = \sum_{j=0}^{5} a_3 \delta_m^j \Delta({}_I\mathbf{d}_j) \quad \text{for } m = 0, 1 \ldots, 5. \tag{79}$$

Next, in order to develop expressions for the tensors $\{{}_I\hat{\mathbf{K}}^{ij}, {}_I\check{\mathbf{K}}^{ij}, {}_I\mathbf{N}^{0j}\}$ it is convenient to introduce additional auxiliary tensors, such that

$$\begin{aligned}
&\Delta({}_I J) = \sum_{j=1}^{5} {}_I\mathbf{a}_0^j \cdot \Delta({}_I\mathbf{d}_j), \quad \Delta({}_I\boldsymbol{\beta}_\alpha) \cdot \mathbf{D}^i = \sum_{j=1}^{5} {}_I\mathbf{a}_\alpha^{ij} \cdot \Delta({}_I\mathbf{d}_j),\\
&\Delta({}_I\mathbf{d}^i) = \sum_{j=1}^{5} {}_I\mathbf{a}_3^{ij} \cdot \Delta({}_I\mathbf{d}_j), \quad \Delta({}_I\mathbf{B}') \cdot {}_I\mathbf{d}^i = \sum_{j=1}^{5} {}_I\mathbf{a}_4^{ij} \cdot \Delta({}_I\mathbf{d}_j), \quad \Delta({}_I\mathbf{B}') \cdot \mathbf{I} = \sum_{j=1}^{5} {}_I\mathbf{a}_5^{j} \cdot \Delta({}_I\mathbf{d}_j),
\end{aligned}$$

$$\Delta({}_I d^{1/2}\,{}_I\mathbf{T})\cdot {}_I\mathbf{d}^i=\sum_{j=1}^{5}{}_I\boldsymbol{\tau}^{ij}\cdot\Delta({}_I\mathbf{d}_j),\quad \Delta({}_I d^{1/2}\,{}_I\hat{\mathbf{T}})\cdot {}_I\mathbf{d}^i=\sum_{j=1}^{5}{}_I\hat{\boldsymbol{\tau}}^{ij}\cdot\Delta({}_I\mathbf{d}_j),$$

$$\Delta({}_I d^{1/2}\,{}_I\check{\mathbf{T}})\cdot {}_I\mathbf{d}^i=\sum_{j=1}^{5}{}_I\check{\boldsymbol{\tau}}^{ij}\cdot\Delta({}_I\mathbf{d}_j),\quad {}_I\boldsymbol{\tau}^{ij}={}_I\hat{\boldsymbol{\tau}}^{ij}+{}_I\check{\boldsymbol{\tau}}^{ij}\quad\text{for }\alpha=1,2\quad\text{and}\quad i=1,2,3\quad\text{and}\quad I=1,2,\ldots,N+1. \tag{80}$$

where the tensors $\{{}_I\mathbf{a}_0^j,{}_I\mathbf{a}_\alpha^{ij},{}_I\mathbf{a}_3^{ij},{}_I\mathbf{a}_4^{ij},{}_I\mathbf{a}_5^j\ \text{for } i=1,2,3 \text{ and } j=1,2,\ldots,5\}$, $\{{}_I\hat{\boldsymbol{\tau}}^{ij},{}_I\check{\boldsymbol{\tau}}^{ij}\}$ are determined presently. Specifically, using the results

$$\begin{aligned}
{}_I\dot{J}&={}_IJ({}_I\mathbf{D}\cdot\mathbf{I})=\left[{}_IJ\sum_{j=1}^{3}{}_I\mathbf{d}^j\right]\cdot{}_I\dot{\mathbf{d}}^j,\quad {}_I\dot{\boldsymbol{\beta}}_\alpha\cdot{}_I\mathbf{D}^i={}_I\mathbf{d}^i\cdot{}_I\dot{\mathbf{d}}_{3+\alpha}+{}_I\dot{\mathbf{d}}^i\cdot{}_I\mathbf{d}_{3+\alpha},\\
{}_I\dot{\mathbf{d}}^i&=-\sum_{j=1}^{3}({}_I\mathbf{d}^i\otimes{}_I\mathbf{d}^j)\cdot{}_I\dot{\mathbf{d}}_j,\\
{}_I\dot{\mathbf{B}}'\cdot{}_I\mathbf{d}^i&=\sum_{j=1}^{3}[\{{}_I\mathbf{B}'\cdot({}_I\mathbf{d}^i\otimes{}_I\mathbf{d}^j)\}\mathbf{I}+{}_I\mathbf{B}'({}_I\mathbf{d}^j\otimes{}_I\mathbf{d}^i)-\frac{2}{3}{}_I\mathbf{B}'({}_I\mathbf{d}^i\otimes{}_I\mathbf{d}^j)]\cdot{}_I\dot{\mathbf{d}}_j,\\
{}_I\dot{\mathbf{B}}'\cdot\mathbf{I}&=\sum_{j=1}^{3}2\left[{}_I\mathbf{B}'-\frac{1}{3}({}_I\mathbf{B}'\cdot\mathbf{I})\cdot\mathbf{I}\right]{}_I\mathbf{d}^j\cdot{}_I\dot{\mathbf{d}}_j\quad\text{for } i,j=1,2,3,
\end{aligned} \tag{81}$$

it follows that

$$\begin{aligned}
&{}_I\mathbf{a}_0^j={}_IJ_I\mathbf{d}^j\ \text{ for } j=1,2,3,\ {}_I\mathbf{a}_0^j=0\quad\text{for}\quad j=4,5,\\
&{}_I\mathbf{a}_1^{ij}={}_I\mathbf{d}_4\otimes{}_I\mathbf{a}_3^{ij},\ {}_I\mathbf{a}_1^{i4}={}_I\mathbf{d}^i+{}_I\mathbf{d}_4\otimes{}_I\mathbf{a}_3^{i4}\quad\text{for } i=1,2,3\quad\text{and}\quad j=1,2,3,5,\\
&{}_I\mathbf{a}_2^{ij}={}_I\mathbf{d}_5\otimes{}_I\mathbf{a}_3^{ij},\ {}_I\mathbf{a}_2^{i5}={}_I\mathbf{d}^i+{}_I\mathbf{d}_5\otimes{}_I\mathbf{a}_3^{i5}\quad\text{for } i=1,2,3\quad\text{and}\quad j=1,2,3,4,\\
&{}_I\mathbf{a}_3^{ij}=-({}_I\mathbf{d}^i\otimes{}_I\mathbf{d}^j),\ {}_I\mathbf{a}_3^{i4}={}_I\mathbf{a}_3^{i5}=0\quad\text{for } i,j=1,2,3,\\
&{}_I\mathbf{a}_3^{ij}=\{{}_I\mathbf{B}'\cdot({}_I\mathbf{d}^i\otimes{}_I\mathbf{d}^j)\}\mathbf{I}+{}_I\mathbf{B}'({}_I\mathbf{d}^j\otimes{}_I\mathbf{d}^i)-\frac{2}{3}{}_I\mathbf{B}'({}_I\mathbf{d}^i\otimes{}_I\mathbf{d}^j),\\
&{}_I\mathbf{a}_4^{i4}={}_I\mathbf{a}_4^{i5}=0\quad\text{for } i,j=1,2,3,\\
&{}_I\mathbf{a}_5^j=2[{}_I\mathbf{B}'-\tfrac{1}{3}({}_I\mathbf{B}'\cdot\mathbf{I})\mathbf{I}]{}_I\mathbf{d}^j,\ {}_I\mathbf{a}_5^4={}_I\mathbf{a}_5^5=0\quad\text{for } j=1,2,3.
\end{aligned} \tag{82}$$

Then, with the help of Eqs. (19), (25), (54) and (80) it can be shown that

$$\begin{aligned}
{}_I\hat{\boldsymbol{\tau}}^{ij}&={}_ID^{1/2}{}_IVK^*{}_I\mathbf{d}^i\otimes{}_I\mathbf{a}_0^j+{}_ID^{1/2}{}_IV\mu^*[{}_I\mathbf{a}_4^{ij}-\tfrac{1}{3}{}_I\mathbf{d}^i\otimes{}_I\mathbf{a}_5^j]\\
&\quad\text{for } i=1,2,3\quad\text{and}\quad j=1,2,\ldots,5,\\
{}_I\hat{\mathbf{K}}^{4j}&={}_ID^{1/2}{}_IV[{}_IL^2\{{}_IK_3{}_I\mathbf{d}^1\otimes{}_I\mathbf{a}_1^{1j}+{}_IK_4{}_I\mathbf{d}^1\otimes{}_I\mathbf{a}_2^{2j}\}\\
&\quad+{}_IW\{{}_IK_6{}_IW_I\mathbf{d}^2\otimes{}_I\mathbf{a}_1^{2j}+{}_IK_7{}_IH_I\mathbf{d}^2\otimes{}_I\mathbf{a}_2^{1j}\}\\
&\quad+{}_IH^2\{{}_IK_1{}_I\mathbf{d}^3\otimes{}_I\mathbf{a}_1^{3j}\}]+{}_ID^{1/2}{}_IV[{}_IL\{{}_IK_3{}_I\kappa_1^1+{}_IK_4{}_I\kappa_2^2\}{}_I\mathbf{a}_3^{1j}\\
&\quad+{}_IW\{{}_IK_6{}_I\kappa_1^2+{}_IK_7{}_I\kappa_2^1\}{}_I\mathbf{a}_3^{2j}+{}_IH\{{}_IK_1{}_I\kappa_1^3\}{}_I\mathbf{a}_3^{3j}],\\
{}_I\hat{\mathbf{K}}^{5j}&={}_ID^{1/2}{}_IV[{}_IH\{{}_IK_7{}_IW_I\mathbf{d}^1\otimes{}_I\mathbf{a}_1^{2j}+{}_IK_8{}_IH_I\mathbf{d}^1\otimes{}_I\mathbf{a}_2^{1j}\}\\
&\quad+{}_IL^2\{{}_IK_4{}_I\mathbf{d}^2\otimes{}_I\mathbf{a}_1^{1j}+{}_IK_5{}_I\mathbf{d}^2\otimes{}_I\mathbf{a}_2^{2j}\}\\
&\quad+{}_IW^2\{{}_IK_2{}_I\mathbf{d}^3\otimes{}_I\mathbf{a}_2^{3j}\}]+{}_ID^{1/2}{}_IV[{}_IH\{{}_IK_7{}_I\kappa_1^2+{}_IK_8{}_I\kappa_2^1\}{}_I\mathbf{a}_3^{1j}\\
&\quad+{}_IL\{{}_IK_4{}_I\kappa_1^1+{}_IK_5{}_I\kappa_2^2\}{}_I\mathbf{a}_3^{2j}+{}_IW\{{}_IK_2{}_I\kappa_2^3\}{}_I\mathbf{a}_3^{3j}]\quad\text{for } j=1,2,\ldots,5.
\end{aligned} \tag{83}$$

For the dissipation terms, Eqs. (11), (12), (40) and (81) are used to rewrite Eq. (26) in the forms

$$
\begin{aligned}
{}_I d^{1/2}\,{}_I\check{\mathbf{T}} &= {}_I D^{1/2}\,{}_I V \sum_{m=1}^{3}[\{{}_I\eta_1 - (2_I\eta_2/3)\}({}_I\mathbf{w}_m \cdot {}_I\mathbf{d}^m)\,\mathbf{I} + 2_I\eta_2({}_I\mathbf{w}_m \otimes {}_I\mathbf{d}^m + {}_I\mathbf{d}^m \otimes {}_I\mathbf{w}_m)],\\
{}_I\check{t}^4 &= {}_I D^{1/2}\,{}_I V[\tfrac{1}{2}{}_I\eta_3\{{}_I\mathbf{d}^2 \cdot {}_I\mathbf{w}_4 - ({}_I\mathbf{d}^2 \cdot {}_I\mathbf{d}_4)\sum_{m=1}^{3}({}_I\mathbf{d}^m \cdot {}_I\mathbf{w}_m)\}{}_I\mathbf{d}^2\\
&\quad + {}_I\eta_4\{{}_I\mathbf{d}^3 \cdot {}_I\mathbf{w}_4 - ({}_I\mathbf{d}^3 \cdot {}_I\mathbf{d}_4)\sum_{m=1}^{3}({}_I\mathbf{d}^m \cdot {}_I\mathbf{w}_m)\} \cdot {}_I\mathbf{d}^3],\\
{}_I\check{t}^5 &= {}_I D^{1/2}\,{}_I V[\tfrac{1}{2}{}_I\eta_3\{{}_I\mathbf{d}^1 \cdot {}_I\mathbf{w}_5 - ({}_I\mathbf{d}^1 \cdot {}_I\mathbf{d}_5)\sum_{m=1}^{3}({}_I\mathbf{d}^m \cdot {}_I\mathbf{w}_m)\}{}_I\mathbf{d}^1\\
&\quad + {}_I\eta_5\{{}_I\mathbf{d}^3 \cdot {}_I\mathbf{w}_5 - ({}_I\mathbf{d}^3 \cdot {}_I\mathbf{d}_5)\sum_{m=1}^{3}({}_I\mathbf{d}^m \cdot {}_I\mathbf{w}_m)\}{}_I\mathbf{d}^3],
\end{aligned}
\tag{84}
$$

so that

$$
\begin{aligned}
{}_I\check{\boldsymbol{\tau}}^{ij} &= {}_I D^{1/2}\,{}_I V\sum_{m=1}^{3}[\{{}_I\eta_1 - (2_I\eta_2/3)\}\{a_1a_3\delta^j_m\,{}_I\mathbf{d}^i \otimes {}_I\mathbf{d}^m + ({}_I\mathbf{d}^i \otimes {}_I\mathbf{w}_m)\,{}_I\mathbf{a}_3^{mj}\}\\
&\quad + 2_I\eta_2\{a_1a_3\delta^i_m({}_I\mathbf{d}^i \cdot {}_I\mathbf{d}^m)\mathbf{I} + ({}_I\mathbf{w}_m \otimes {}_I\mathbf{d}^i)\,{}_I\mathbf{a}_3^{mj} + ({}_I\mathbf{d}^i \cdot {}_I\mathbf{w}_m)\,{}_I\mathbf{a}_3^{mj}\\
&\quad + a_I a_3\delta^j_m({}_I\mathbf{d}^m \otimes {}_I\mathbf{d}^i)] \quad \text{for } i,m = 1,2,3 \quad \text{and} \quad j = 1,2,\ldots,5,
\end{aligned}
$$

$$
\begin{aligned}
{}_I\check{\mathbf{K}}^{4j} &= \tfrac{1}{2}{}_I\eta_3\,{}_I D^{1/2}\,{}_I V[({}_I\mathbf{d}^2 \otimes {}_I\mathbf{w}_4)\,{}_I\mathbf{a}_3^{2j} + a_1a_3\delta^j_4({}_I\mathbf{d}^2 \otimes {}_I\mathbf{d}^2)\\
&\quad - \sum_{m=1}^{3}({}_I\mathbf{d}^m \cdot {}_I\mathbf{w}_m)\{({}_I\mathbf{d}^2 \otimes {}_I\mathbf{d}_4)\,{}_I\mathbf{a}_3^{2j} + \delta^j_4({}_I\mathbf{d}^2 \otimes {}_I\mathbf{d}^2)\}\\
&\quad - ({}_I\mathbf{d}^2 \cdot {}_I\mathbf{d}_4)\sum_{m=1}^{3}\{({}_I\mathbf{d}^2 \otimes {}_I\mathbf{w}_m)\,{}_I\mathbf{a}_3^{mj} + a_1a_3\delta^j_m({}_I\mathbf{d}^2 \otimes {}_I\mathbf{d}^m)\}]\\
&\quad + \{{}_I\mathbf{d}^2 \cdot {}_I\mathbf{w}_4 - ({}_I\mathbf{d}^2 \cdot {}_I\mathbf{d}_4)\sum_{m=1}^{3}({}_I\mathbf{d}^m \cdot {}_I\mathbf{w}_m)\}{}_I\mathbf{a}_3^{2j}]\\
&\quad + {}_I\eta_4\,{}_I D^{1/2}\,{}_I V[({}_I\mathbf{d}^3 \otimes {}_I\mathbf{w}_4)\,{}_I\mathbf{a}_3^{3j} + a_1a_3\delta^j_4({}_I\mathbf{d}^3 \otimes {}_I\mathbf{d}^3)\\
&\quad - \sum_{m=1}^{3}({}_I\mathbf{d}^m \cdot {}_I\mathbf{w}_m)\{({}_I\mathbf{d}^3 \otimes {}_I\mathbf{d}_4)\,{}_I\mathbf{a}_3^{3j} + \delta^j_4({}_I\mathbf{d}^3 \otimes {}_I\mathbf{d}^3)\}\\
&\quad - ({}_I\mathbf{d}^3 \cdot {}_I\mathbf{d}_4)\sum_{m=1}^{3}\{({}_I\mathbf{d}^3 \otimes {}_I\mathbf{w}_m)\,{}_I\mathbf{a}_3^{mj} + a_1a_3\delta^j_m({}_I\mathbf{d}^3 \otimes {}_I\mathbf{d}^m)\}\\
&\quad + \{{}_I\mathbf{d}^3 \cdot {}_I\mathbf{w}_4 - ({}_I\mathbf{d}^3 \cdot {}_I\mathbf{d}_4)\sum_{m=1}^{3}({}_I\mathbf{d}^m \cdot {}_I\mathbf{w}_m)\}{}_I\mathbf{a}_3^{3j}],
\end{aligned}
$$

$$
\begin{aligned}
{}_I\check{\mathbf{K}}^{5\mathrm{j}} &= \tfrac{1}{2}{}_I\eta_3\,{}_I D^{1/2}\,{}_I V[({}_I\mathbf{d}^1 \otimes {}_I\mathbf{w}_5)\,{}_I\mathbf{a}_3^{1\mathrm{j}} + a_1a_3\delta^j_5({}_I\mathbf{d}^1 \otimes {}_I\mathbf{d}^1)\\
&\quad - \sum_{m=1}^{3}({}_I\mathbf{d}^m \cdot {}_I\mathbf{w}_m)\{({}_I\mathbf{d}^1 \otimes {}_I\mathbf{d}_5)\,{}_I\mathbf{a}_3^{1j} + \delta^j_5({}_I\mathbf{d}^1 \otimes {}_I\mathbf{d}^1)\} - ({}_I\mathbf{d}^1 \cdot {}_I\mathbf{d}_5)\\
&\quad \times \sum_{m=1}^{3}\{({}_I\mathbf{d}^1 \otimes {}_I\mathbf{w}_m)\,{}_I\mathbf{a}_3^{mj} + a_1a_3\delta^j_m({}_I\mathbf{d}^1 \otimes {}_I\mathbf{d}^m)\} + \{{}_I\mathbf{d}^1 \cdot {}_I\mathbf{w}_5 - ({}_I\mathbf{d}^1 \cdot {}_I\mathbf{d}_5)
\end{aligned}
$$

$$\times \sum_{m=1}^{3} ({}_I\mathbf{d}^m \cdot {}_I\mathbf{w}_m)\}{}_I\mathbf{a}_3^{1j}] + {}_I\eta_5 {}_ID^{1/2} {}_IV[({}_I\mathbf{d}^3 \otimes {}_I\mathbf{w}_5){}_I\mathbf{a}_3^{3j} + a_1a_3\delta_5^j({}_I\mathbf{d}^3 \otimes {}_I\mathbf{d}^3)$$

$$- \sum_{m=1}^{3} ({}_I\mathbf{d}^m \cdot {}_I\mathbf{w}_m)\{({}_I\mathbf{d}^3 \otimes {}_I\mathbf{d}_5){}_I\mathbf{a}_3^{3j} + \delta_5^j({}_I\mathbf{d}^3 \otimes {}_I\mathbf{d}^3)\} - ({}_I\mathbf{d}^3 \cdot {}_I\mathbf{d}_5)$$

$$\times \sum_{m=1}^{3} \{({}_I\mathbf{d}^3 \otimes {}_I\mathbf{w}_m){}_I\mathbf{a}_3^{mj} + a_1a_3\delta_m^j({}_I\mathbf{d}^3 \otimes {}_I\mathbf{d}^m)\} + \{{}_I\mathbf{d}^3 \cdot {}_I\mathbf{w}_5 - ({}_I\mathbf{d}^3 \cdot {}_I\mathbf{d}_5)$$

$$\times \sum_{m=1}^{3} ({}_I\mathbf{d}^m \cdot {}_I\mathbf{w}_m)\}{}_I\mathbf{a}_3^{3j}] \quad \text{for } j = 1, 2, \ldots, 5. \tag{85}$$

Next, with the help of Eqs. (13), (25), (26), (54) and (80), it can be seen that the tensors $\{{}_I\mathbf{K}^{ij}, {}_I\hat{\mathbf{K}}^{ij}, {}_I\check{\mathbf{K}}^{ij}$ for $i = 1, 2, 3\}$ all satisfy equations of the forms

$${}_I\mathbf{K}^{ij} = {}_I\boldsymbol{\tau}^{ij} - ({}_I\mathbf{d}_4 \cdot {}_I\mathbf{d}^i){}_I\mathbf{K}^{4j} - ({}_I\mathbf{t}^4 \otimes {}_I\mathbf{d}^i)\delta_4^j - ({}_I\mathbf{d}_5 \cdot {}_I\mathbf{d}^i){}_I\mathbf{K}^{5j} - ({}_I\mathbf{t}^5 \otimes {}_I\mathbf{d}^i)\delta_5^j$$
$$+ ({}_Id^{1/2} {}_I\mathbf{T} - {}_I\mathbf{t}^5 \otimes {}_I\mathbf{d}_4 - {}_I\mathbf{t}^5 \otimes {}_I\mathbf{d}_5){}_I\mathbf{a}_3^{ij} \quad \text{for } i = 1, 2, 3 \text{ and } j = 1, 2, \ldots, 5. \tag{86}$$

Finally, using Eq. (28) it can be shown that

$$\Delta({}_Im_I\mathbf{B}^0) = -{}_IC_D\rho_aA\left[\left\{\frac{{}_I\mathbf{w}_0}{|{}_I\mathbf{w}_0|} \cdot \Delta({}_I\mathbf{w}_0)\right\}{}_I\mathbf{w}_0 + |{}_I\mathbf{w}_0|\Delta({}_I\mathbf{w}_0)\right],$$

$${}_I\mathbf{N}^{0j} = -a_1a_3C_D\rho_aA\left[\left\{{}_I\mathbf{w}_0 \otimes \frac{{}_I\mathbf{w}_0}{|{}_I\mathbf{w}_0|}\right\} + |{}_I\mathbf{w}_0|\mathbf{I}\right]\delta_0^j \quad \text{for } j = 0, 1, \ldots, 5. \tag{87}$$

References

[1] O. Yogev, I. Bucher, M.B. Rubin, Dynamic lateral torsional post-buckling of a beam–mass system: experiments, *Journal of Sound and Vibration* 299 (2007) 1049–1073.

[2] S.S. Antman, *The Theory of Rods, Handbuch der Physik*, Vol. VIa/2, Springer, Berlin, 1972.

[3] S.S. Antman, *Nonlinear Problems of Elasticity*, Springer, New York, 1995.

[4] A.E. Green, P.M. Naghdi, M.L. Wenner, On the theory of rods I: derivations from the three-dimensional equations, *Proceedings of the Royal Society of London A* 337 (1974) 451–483.

[5] A.E. Green, P.M. Naghdi, M.L. Wenner, On the theory of rods II: developments by direct approach, *Proceedings of the Royal Society of London A* 337 (1974) 485–507.

[6] M.R.M.C. Da Silva, C.L. Zaretzky, D.H. Hodges, Effects of approximations on the static and dynamic response of a cantilever with a tip mass, *International Journal of Solids and Structures* 27 (1991) 565–583.

[7] J.C. Simo, L. Vu-Quoc, On the dynamics of flexible beams under large overall motions—the plane case—part II, *ASME Journal of Applied Mechanics* 53 (1986) 855–863.

[8] J.C. Simo, L. Vu-Quoc, A three-dimensional finite strain rod model—part II. Computational aspects, *Computer Methods in Applied Mechanics and Engineering* 58 (1986) 79–116.

[9] J.C. Simo, L. Vu-Quoc, On the dynamics in space of rods undergoing large motions—a geometrically exact approach, *Computer Methods in Applied Mechanics and Engineering* 66 (1988) 125–161.

[10] J.C. Simo, A finite strain beam formulation. The three-dimensional dynamic problem—part I, *Computer Methods in Applied Mechanics and Engineering* 49 (1985) 55–70.

[11] M.B. Rubin, *Cosserat Theories: Shells, Rods and Points, Solid Mechanics and its Applications*, Vol. 79, Kluwer, The Netherlands, 2000.

[12] M.B. Rubin, Numerical solution procedures for nonlinear elastic rods using the theory of a Cosserat point, *International Journal of Solids Structures* 38 (2001) 4395–4437.

[13] B. Nadler, M.B. Rubin, Post-buckling behavior of nonlinear elastic beams and three-dimensional frames using the theory of a Cosserat point, *Mathematics and Mechanics of Solids* 9 (2004) 369–398.

[14] M.B. Rubin, Buckling of elastic shallow arches using the theory of a Cosserat point, *Journal of Engineering Mechanics—ASCE* 130 (2004) 216–224.

[15] M.B. Rubin, E. Tufekci, Three-dimensional free vibrations of a circular arch using the theory of a Cosserat point, *Journal of Sound and Vibration* 286 (2005) 799–816.

[16] B. Nadler, M.B. Rubin, Determination of hourglass coefficients in the theory of a Cosserat point for nonlinear elastic beams, *International Journal of Solids and Structures* 40 (2003) 6163–6188.
[17] P. Flory, Thermodynamic relations for high elastic materials, *Transactions of the Faraday Society* 57 (1961) 829–838.
[18] R.W. Fox, A.T. Mcdonald, *Introduction to Fluid Mechanics*, fifth ed., Wiley, New York, 1998.
[19] ANSYS Release 8.1, ANSYS Inc., Cannonsburg, PA.